Chapter 4

Preparation and Characterization of Highly Porous Soy Protein Cryogel for Skin Tissue Engineering

4.1 Introduction

SPI is a highly abundant plant protein-polymer that has several remarkable properties such as excellent biocompatibility, biodegradability, good hydrophilicity, and hence has attracted keen attention as a replacement for synthetic polymers as well as polymers of animal origin. Albeit this, the inferior mechanical performance of pure SPI limits its widespread applicability in TE applications. However, it has numerous reactive groups such as -OH, -SH, -NH2, and –COOH and hence its mechanical strength can be increased by physical and chemical modification or crosslinking reactions. In particular, chemicals from the aldehyde family, such as GA or formaldehyde can be employed as cross-linking agents. These aldehydes mainly react with the basic group of lysine, hydroxylysine arginine, and histidine residues of the protein to form a cross-linked structure by making inter and intramolecular cross-links (Peles and Zilberman 2012). GA is one of the most commonly used cross-linking agents, but some concerns regarding its cytotoxicity have been raised due to the release of monomers during the application (Huang-Lee, Cheung, and Nimni 1990). To neutralise the harmful and adverse effects of residual GA after crosslinking, the GA-cross-linked polymer is frequently washed with a glycine-containing solution (Yang et al. 2018). However, some studies have also found that at low concentrations of GA, there is no toxic effect on cells. Particularly, Curt et al. employed various concentrations of formaldehyde i.e., 0, 1, 2, and 3%, as a crosslinking agent to improve the mechanical characteristics of SPI films. The stability of the formed films was improved due to decreased water absorption by increasing the amount of formaldehyde. In vitro investigations revealed that the use of formaldehyde had no harmful effects and had no detrimental impact on the attachment, growth and viability, of human fibroblast and keratinocyte cells (Curt, Subirade, and Rouabhia 2009). In a work by Ramnath et al., temporary wound-dressing materials were made from composite

biomaterials made from soy protein and sago starch cross-linked with GA and observed enhanced wound healing after treatment in comparison to control (Ramnath et al., 2012). Ghorpade et al. reported a two-fold increase in the tensile strength (TS) and puncture strength of soy proteins films after crosslinking with formaldehyde (S. K. Park, Bae, and Rhee 2000).

Several techniques have been employed in the literature to fabricate complex 3D structures. These include electrospinning, solvent casting, freeze drying, salt leaching, phase separation, melt moulding, and gas foaming. Among them, freeze-drying is one such technique that is often employed for manufacturing scaffolds for TE purposes. However, this technique suffers from some drawbacks such as the inability to control pore size, inconsistent pore distribution, and inferior mechanical properties. These limitations can be overcome by employing cryogelation technique. It is a gelation process that takes place in semi-frozen conditions and yields a cross-linked polymer network surrounding the ice crystals. Moreover, using this technique cryogels can be prepared in a variety of sizes and formats, including discs, sheets, and monoliths with varied dimensions, which makes the cryogelation approach superior to conventional fabrication procedures (Y. Liu et al. 2014). Furthermore, in comparison to the conventional methods, this technique offers the formation of highly porous structure with better mechanical properties. Moreover, it is a more advantageous technique than others used for the fabrication of porous scaffolds, such as phase separation paired with freeze-drying or particulate leaching/solvent casting since it does not involve the use of organic solvents or other additives during the process of manufacturing. Also, it is a more cost-efficient technique in comparison to the commonly used freeze-drying technique (Dainiak et al. 2010). Moreover, cryogel matrices have also been used in bioreactors for monoclonal antibody synthesis, affinity chromatographic separations, cell chromatography, and cell

separation, in addition to TE (Patro and Wagner 2016; Mansur et al. 2008; He et al. 2021; Lozinsky 2002).

In this chapter, chemically cross-linked SPI hydrogels with large and interconnected microporous structure of different polymer concentrations were synthesized under sub-zero conditions using the cryogelation technique. The prepared samples were characterized physically, chemically, and mechanically in terms of in vitro degradation rate, TGA analysis, DSC analysis, FTIR, and cyclic compression. SEM micrographs were used to examine the morphology of all the prepared hydrogels. Furthermore, the effect of polymer concentration on pore size, porosity, and swelling was also examined. Blood hemocompatibility of SPI cryogels was also evaluated. A direct contact cytotoxicity test was performed to study the potential toxicity of the materials and their degraded products towards mammalian cells and also evaluate the ability of scaffolds to promote cell infiltration, adherence, growth, and proliferation. This work also explored the efficacy of SPI cryogels as a potential wound dressing material.

4.2 Materials and methods

4.2.1 Materials

Soy protein isolate powder of A.M. NUTRATECH Pvt. Ltd., India, was used in this work. High glucose DMEM, trypsin-EDTA solution, FBS, PFA, PBS, antibiotics penicillin and streptomycin solution, trypan blue, MTT assay kit, DAPI, trypan blue, triton X-100 and DMSO of HiMedia, India, were used. Centrifuge tubes (15 and 50 mL) and multi well plates (96 and 12 well plate) of GENETIX, 25% GA of Loba Chemie and petri dishes non-culture grade (35 mm) of TARSON were utilized. High analytical grade ethanol and pure distilled water were utilized.

4.2.2 Synthesis of cryogels

GA cross-linked soy protein superporous cryogels were prepared through cryogelation technique. SPI cryogels with different polymer concentration (w/v) were fabricated viz. 2% SPI, 4% SPI, 6% SPI, 8% SPI and 10% SPI (Table 4.1). In brief, the homogenous solutions of different concentration of SPI were prepared in distilled water. For making this solution, SPI powder of given concentration was added in water and the obtained solution was continuously stirred at 60˚C for an hour. After that, the temperature of the obtained homogenous solution was brought down to room temperature and then poured into pre-cooled syringe moulds. Thereafter, 1% GA solution was added to the SPI solutions and gently mixed by repeatedly inverting the closed moulds. This was followed by freezing the solution at -12 ˚C for 24 h and then thawing it at room temperature. During the freezing process, the liquid component of the solution is gets converted to ice crystals, and during thawing, these ice crystals melt and leave interconnected pores in the structure. The formed cross-linked hydrogels were then washed several times with distilled water to remove any remaining non-reacted GA. Additionally, to evaluate the temperature influence on the gel formation, the respective solutions with the same SPI and GA ratios were likewise formed and incubated at room temperature and 0 ˚C for 24 h. A schematic of the fabrication process of SPI cryogels and the prepared cryogel images are presented in Figure 4.1, and Figure 4.2, respectively.

Table 4.1 Formulations of various fabricated SPI cryogels.

Sample (w/v)	GA (%)	SPI (g)	Water (mL)
10% SPI	1.00	1.00	10
8% SPI	1.00	0.80	10
6% SPI	1.00	0.60	10
4% SPI	1.00	0.40	10
2% SPI	1.00	0.20	10

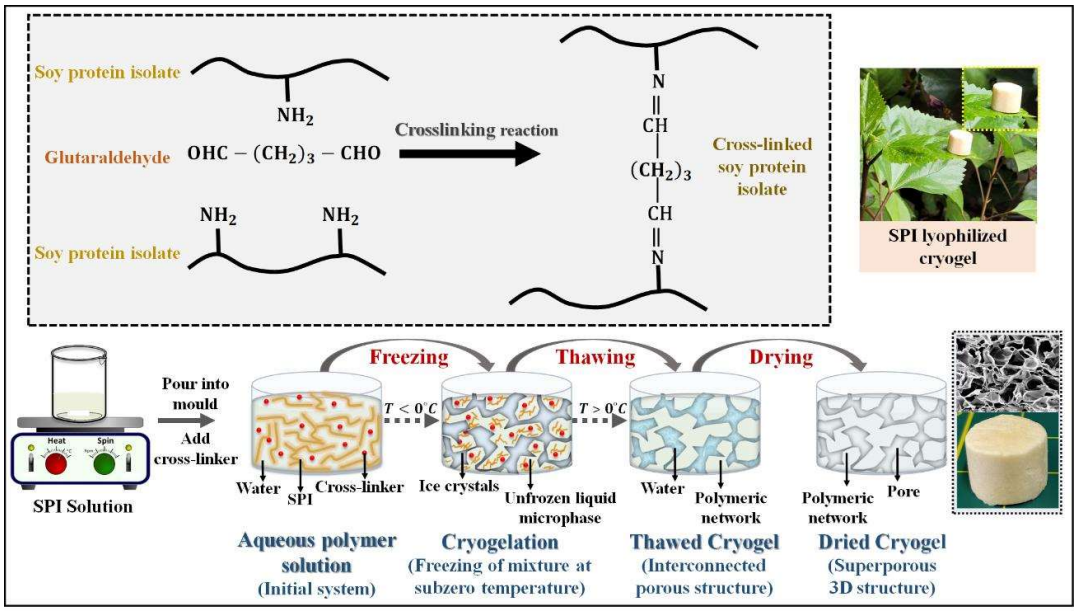

Figure 4.1 Schematic representation of the fabrication process of GA cross-linked superporous SPI scaffolds using cryogelation technique.

4.2.3 Characterization of the cryogels

4.2.3.1 Morphological analysis

The topographical and microstructure analysis of prepared samples were investigated by using optical ((Nikon Ti-U) fluorescence microscope) and SEM (Zeiss EVO 18 SEM Zeiss, Oberkochen, Germany). SEM was used to determine the internal morphology and

pore size distribution of the samples. The lyophilized cryogel samples were coated with gold at 20 kV for SEM imaging. In order to investigate the distribution of pore sizes in the samples, the obtained micrographs were analysed with the ImageJ software.

4.2.3.2 Porosity

Using the liquid replacement approach, the porosity of synthesized lyophilized cryogels was determined. The cylindrical samples were first weighed (W_D) and then soaked in 100% EtOH. Absolute ethanol was chosen as the replacement liquid since it penetrates through the scaffolds without causing any expansion or contraction of the matrix. Using numerous evacuation-repressurization cycles in a vacuum desiccator, all submerging samples were exposed to ethanol penetration. The saturated hydrogels' weight was designated as W_W. The porosity was estimated using the expression in Equations (3.2) and (3.3).

4.2.3.3 Swelling capacity

The ability of wound dressings to absorb fluid is crucial for their effectiveness in treatment of chronic wounds. The cryogels' water absorption capacity and saturation state were measured by immersing the pre-weighed lyophilized samples in PBS solution (with a pH of 7.4) for 48 h at room temperature. A precise electronic weighing balance was used to weigh samples prior to and post-immersion at predetermined intervals. Filter paper was used to gently remove excess water from the sample's surface and it was then weighed. The swelling (%) was determined using the expression in Equation (2.1).

Fluid uptake capacity is one of the important requirement of a wound dressing in order to provide a moist environment that promotes rapid wound healing. After reaching equilibrium, the MWC was determined using the expression in Equation (3.4).

4.2.3.4 Water retention studies

The cryogels were evaluated for water retention in accordance with the literature (Qi et al. 2015). Before the water retention experiments, the cryogel tubes were allowed to swell in distilled water (room temperature) until they reached equilibrium. Then, the water-saturated cryogel samples were incubated at 37° C in an oven and weighed as they collapsed at set times. The hydrogels' water retention (W_r) was calculated as follows:

$$W_r\ (\%) = \left(\frac{W_t}{W_s}\right) \times 100, \tag{4.1}$$

where W_t denotes the weight of the SPI cryogel sample at various time points throughout the shrinking process and W_s denotes the weight of the water-saturated cryogels at equilibrium.

4.2.3.5 In vitro degradation study

By immersing the cryogels in PBS solution (with a pH of 7.4) and lysozyme solution (10^4 U/ mL) at 37 °C, the degradation rate of lyophilized cryogel scaffolds was investigated. The weight (W_i) of lyophilized scaffolds was determined before immersion in the appropriate solutions. The degradation of materials was studied during a 12-day period, with the solution being replenished every two days. At the end of the experiment on the 12^{th} day, samples were removed from the solution and rinsed three times with distilled water. The weight loss percentage of the scaffolds was estimated mathematically using the expression in Equation (2.2).

4.2.3.6 FTIR

The infrared spectra of the SPI cryogel samples were recorded using an ALPHA BRUKER Eco-ATR (with a ZnSe-attenuated total reflection (ATR) accessory)

instrument. For each spectrum, a total of 24 scans with a resolution of 4 cm^{-1} were acquired in the infrared spectrum between 500 and 3500 cm^{-1}.

4.2.3.7 TGA

The TGA was carried out on a Shimadzu (Asia Pacific) Pte. Ltd. TGA-50 thermogravimetric analyzer. The experiment was conducted at temperatures ranging from 20 to 500 ˚C, with a heating rate of 10 ˚C per minute. The thermal stability of the material was determined using TGA by tracking the change in weight over time and temperature.

4.2.3.8 DSC

The thermal behaviour of prepared lyophilized cryogels was investigated using DSC (Mettler STAR SW 10.00 instrument) in an N_2 environment. Before usage, the instrument was calibrated with indium. The T_g and T_m were determined using the DSC thermograms from the second heating run (heating rate: 10 °C/min and average N_2 gas flow rate: 55 mL min^{-1}).

4.2.3.9 Mechanical evaluation of the SPI cryogels

The mechanical assessment of each scaffold is essential because, for feasible and long-term therapeutic applications, they should have appropriate handling properties as well as enough resistance to deformation and breakage. Therefore, compression experiments were conducted using a Texture Analyzer (Shimadzu) under axial compression with a 500 N load cell at a loading speed of 0.5 mm/sec to examine the mechanical strength of chemically cross-linked SPI cryogels. Compressive testing was used to examine tubular shaped wet (with PBS solution) samples with dimensions of 1.5 cm in height and 1.4 cm in diameter. At 50% and 80% compression, the stiffness of every cryogel was measured in triplicates. The average slope of the linear section of the generated stress vs strain graph

was used to compute the compressive modulus. Furthermore, to assess the high resilience with swift recovery and strength of the highly porous SPI cryogels, the dynamic stress-strain behaviour of the prepared SPI cryogels was carried out for 10 cycles with two different strains of 50%, and 80%.

4.2.3.10 Shape memory of SPI cryogels

The cryogels' shape memory properties were tested according to (Zhao et al. 2018). At a strain rate of 0.5 mm/s, the prepared SPI cryogel with an original length of 15 mm (L_1) was compressed up to 80% strain and held for 1 minute. The water wringed out from the compressed cryogel was then totally absorbed using paper, and the obtained compressed length was measured as L_2. After 5 minutes of being free from any load, the sample fixed was measured as L_3. The sample was then immersed in water for 1 minute to rehydrate it, and the recovered sample length was set to L_4. A Shimadzu Texture Analyzer was used to conduct the test. The L_2 was automatically measured by the instrument, whereas L_1, L_3, and L_4 were manually measured using digital Vernier calliper. The test was repeated three times at least. The following equations were used to compute the shape memory fixity ratio and recovery ratio:

$$Maximaum\ compresssive\ starin\ (\%)\ \varepsilon_m = \left(\frac{L_1 - L_2}{L_1}\right) \times 100, \quad \textbf{(4.2)}$$

$$Fixed\ strain\ (\%)\ \varepsilon_f = \left(\frac{L_1 - L_3}{L_1}\right) \times 100, \quad \textbf{(4.3)}$$

$$Recovery\ strain\ (\%)\ \varepsilon_r = \left(\frac{L_4 - L_3}{L_1}\right) \times 100, \quad \textbf{(4.4)}$$

$$Strain\ fixity\ ratio\ (\%)\ R_f = \left(\frac{\varepsilon_f}{\varepsilon_m}\right) \times 100, \quad \textbf{(4.5)}$$

$$Strain\ recovery\ ratio\ (\%)\ R_r = \left(\frac{\varepsilon_r}{\varepsilon_f}\right) \times 100. \quad \textbf{(4.6)}$$

4.2.3.11 Volumetric expansion ratios of the SPI cryogels

The shape-free diameter (d_1) and length (l_1) of columniform sample were examined before the shape was fixed. To obtain the shape-fixed sample, the free water in the columniform sample was squeezed out. The shape-fixed sample's diameter (d_2) and length (l_2) were then measured. The following equation was used to compute the volumetric expansion ratio (V_E):

$$V_E = \frac{\left(\frac{d_1}{2}\right)^2 \times l_1}{\left(\frac{d_2}{2}\right)^2 \times l_2}. \quad \textbf{(4.7)}$$

4.2.3.12 Whole blood cell adhesion test on SPI cryogels

The prepared cryogel samples were cut into small size discs and incubated for 1 h at 37 ˚C. After that, the whole blood was added dropwise onto the samples and placed for 5 minutes at 37°C. The samples were then rinsed three times with PBS to eliminate any physically adherent blood cells. The cryogels were then fixed by 4% paraformaldehyde for an hour. Thereafter, the blood cells were serially dehydrated with 50% → 60% → 70% → 80% → 90% → 100% ethanol solution. SEM was used to examine the morphology of hemocytes on cryogel samples.

4.2.3.13 Haemolytic activity test on SPI cryogels

The relative quantities of haemoglobin released into solution phase from erythrocytes in whole blood subjected to the test materials were used to assess haemolytic activity according to (Y. Liu et al. 2014). For the study, fabricated SPI cryogel samples (4%, 6%

and 8%) were cut into cylindrical shape (diameter = 10 mm, height = 5 mm). Sterile samples were then washed with PBS solution for three times. The anticoagulated diluted blood (10 mL of PBS + 8 mL of anticoagulated blood) was used as a source of haemoglobin. Test tubes containing cryogel samples with 10 mL PBS was taken as test group. 10 mL PBS was considered as a negative control while 10 mL distilled water was taken as a positive control to produce maximum erythrocyte lysis. All test tubes were warmed for 30 minutes in a 37 °C constant-temperature water bath, then 0.2 mL diluted anticoagulated fresh whole blood was added and the tubes were returned to the water bath for another 60 min. The test tubes were centrifuged at 100 × g for 5 min after the second incubation period. The absorbance of the supernatant containing the solubilized haemoglobin was measured at a wavelength of 540 nm (O.D.). The following formula was used to determine the degree of hemolysis (%) using the average O.D. value:

$$Hemolysis\ (\%)\ =\ \left[\frac{(Ab_s - Ab_n)}{(Ab_p - Ab_n)}\right] \times 100, \qquad \textbf{(4.8)}$$

where Ab_s, Ab_n and Ab_p denote the absorbance of supernatant of test samples, PBS (negative control) and distilled water (positive control), respectively.

4.2.3.14 Whole blood clotting of the SPI cryogels

The cryogels were evaluated for whole-blood coagulation in accordance with the literature (Zhao et al. 2018). The cylindrical shape cryogels with a height of 5 mm and a diameter of 8 mm, were used for the study. In polypropylene tubes, a volume of 60 µL of recalcified whole-blood solution (0.2 M $CaCl_2$, 10 mM in the blood) was added to the prewarmed cryogels (37 °C). The tubes were then incubated for different durations of 1,2,3,4 and 5 min, at 37 °C. The control groups were gauze and cotton. 10 mL distilled water was gently added after the pre-set duration to remove unbound blood without

disrupting the clot. Using a microplate reader, the absorbance of the supernatant was measured at 540 nm (Molecular Devices). The absorbance of 60 µL of recalcified whole blood in 10 mL of distilled water was taken as the reference value. This was set as the negative control. The following equation was used to determine the blood-clotting index (BCI):

$$BCI\ (\%)\ =\ \left[\frac{(Ab_s - Ab_w)}{(Ab_r - Ab_w)}\right] \times 100, \qquad \textbf{(4.9)}$$

where Ab_s, Ab_w, and Ab_r represent the absorbance of sample, distilled water and negative control (reference value), respectively.

4.2.3.15 Cytocompatibility study

4.2.3.15.1 Microscopic analysis

For cell culture experiments, the L929 cell line, which is a mouse fibroblast cell, was used. The cells were maintained in a CO_2 incubator (Galaxy® 170 S, Eppendorf, Germany) with a complete growth medium comprising of DMEM supplemented with 10% of FBS and 1% of PS at 37°C, 5% CO_2, and 95% humidity. The lyophilized cryogels were preincubated in a 35-mm Petri dish with complete growth medium for 60 min. The extra medium was withdrawn and discarded after preincubation, and the samples were allowed to dry in an incubator for 30 minutes. The samples were then seeded with 1×10^5 cells and left for an hour at 37 °C in a CO_2 incubator to provide cell attachment. Thereafter, the plates were filled with 2 mL of complete culture media and then placed in the CO_2 incubator for continued incubation. Samples were moved routinely to a new Petri plate during fluorescent microscopic imaging to avoid fluorescence interference caused by cells that had migrated and attached to the surface of the wells.

SEM was used to analyse the adherence and morphology of cells on the cell-cultured SPI cryogels. After 6 days of culture, the cryogel samples were rinsed in PBS solution and

then fixed with 4% PFA. The cell-seeded cryogel samples were then sequentially dehydrated as explained in section "4.2.3.12" and thereafter the samples were air-dried overnight. For SEM analysis, all dried cryogel samples were coated with gold.

4.2.3.15.2 MTT assay

The MTT reduction test was conducted to assess the cell viability of L929 cells within the SPI cryogels. The test was carried out on samples with a diameter of 4 mm placed in the 96-well plate's wells. For sterilization, the lyophilized SPI cryogel samples were first exposed to ultra-violet radiation for an hour. Following that, the cells were seeded at a density of 10^4 cells/ sample. The samples were then placed in a CO_2 incubator for two to four days. The cells cultured in wells without scaffolds were considered a positive control, and only complete growth medium was kept as a negative control.

4.2.3.16 In vivo wound healing assay

The prepared SPI cryogels were examined in full-thickness wound excision rat models for in vivo wound healing. The experiment was carried out after receiving clearance from Banaras Hindu University's Central Animal Ethical Committee (CAEC) (No. Dean/2018/CAEC/804). An intraperitoneal dose of ketamine (35 mg/kg) and xylazine (5–10 mg/kg) was used to anesthetize a total of nine adult Wistar rats (age: 5-7 months) weighing 150–250 g. Hairs on the dorsal side were trimmed, and the skin surface was cleansed with ethanol solution. Following that, skin excision was used to create a circular full-thickness wound with a diameter of around 12 mm. The rats were divided into three groups at random: one group received treatment of 4% SPI cryogels, another received treatment of 6% SPI cryogels, and the third group received no treatment, i.e., sham. Three rats (n = 3) were there in each group. Images were captured using a digital camera at regular intervals. The wound area was marked on a transparent sheet and measured

with graph paper. The wound closure rate was estimated using the expression in Equation (2.3).

After 16 days, the skin was dissected and fixed with 4% formalin. The samples were then sequentially dehydrated using different EtOH concentrations and trimmed into small slices before being permeated with liquid paraffin. The paraffin-permeated sample slices were then implanted in paraffin-containing molds to form tissue blocks. Blocks were sectioned into 5 µm thick slices with a microtome. After that, these sections were mounted on the slides, and then H&E staining was performed. An OLYMPUS bright-field (upright) microscope was used to examine the obtained slides. ToupView 3.7 software was used to view and record the images.

4.2.3.17 Statistical analysis

The experiments were carried out in triplicate, and the results were represented as mean ± SD. For statistical analysis, ANOVA with Tukey's multiple comparison tests was performed for all the experimental data. OriginPro 2020 (OriginLab, Learning edition) was used to plot all the graphs. In fluorescence images, the background noise was subtracted using ImageJ software. To convolve the image, the Gaussian blur function was employed followed by image subtraction to remove the background noise.

4.3 Results

4.3.1 Morphological analysis of the prepared SPI cryogels

The SPI solution was chemically cross-linked by using cryogelation technique. 1% (v/v) GA was used to get water insoluble, stable and mechanically robust hydrogels. The obtained cryogels were transparent, soft, flexible and light yellow in colour (Figure 4.2 (a)). From the digital images, it was observed that 2% SPI and 10% SPI samples were unable to retain their uniform morphology due to very low and high concentration of polymer in comparison to crosslinking agents, respectively. The obtained cryogels were

found to be very light weighted because of the superporous structure (Figure 4.2(b)). In addition, the same initial solution of SPI and GA was unable to form the cross-linked structure at 0 ˚C or positive temperatures. Microstructure analysis was performed using SEM micrographs. All the prepared SPI cryogels were found to be highly porous with open pore interconnected mesh like architecture (Figure 4.3). However, 10% SPI was found to have non-uniform porous structure. The pores in the 10% SPI cryogel scaffolds ranged from 5 to 443 μm, with an average pore size of 79.6 ± 62 μm, although the majority of them ranged from 10 to 250 μm. Pore sizes ranged between 3 and 308 μm in 8 % SPI scaffolds. The average pore size was 45.79 ± 35.3 μm, with the majority of them falling between 10 and 200 μm. The 6% scaffolds had a minimum pore size of 4.35 μm and a maximum pore size of 491 μm. For this concentration, the average pore size was 53.7 ± 46.2 μm, with the majority falling between 10 and 200 μm. In 4% cryogels, the extent of pore size was determined to be 4.8–690 μm, with an average pore size of 92.67 ± 87.5 μm and majority of them lying in the range of 12–350 μm. While the 2% cryogels had pore sizes ranging from 12 to 419 μm with an average pore size of 87.69 ± 59.6 μm, the majority of the pores were between 14 and 300 μm. We obtained chemically cross-linked network of soy protein with pore size in micrometre range. When the polymer concentration was increased, the pores in the scaffolds appeared to be tightly packed, which resulted in comparatively small pore sizes. The interconnectivity of the pores was clearly visible in SEM micrographs at high magnification for all the samples. 2% SPI samples showed a reduced average pore size than the 4% SPI samples because of the inability of the former to maintain the structure after lyophilisation due to very low polymer concentration. In contrast, the average pore size in 10% SPI samples was found to be larger than the pore sizes obtained for 6% and 8% SPI samples. This might be

because of the non-uniform structure formation during the cryogelation process due to the higher polymer concentration.

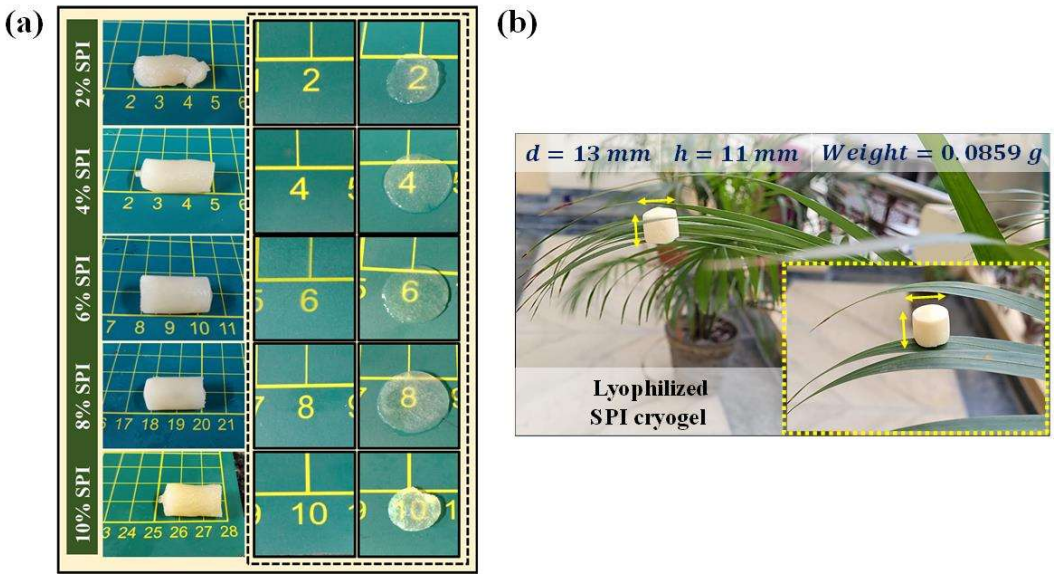

Figure 4.2 Digital images of **(a)** all the prepared SPI cryogels after thawing and their respective disc shaped section showing transparency property of the samples and **(b)** light-weight prepared cylindrical SPI cryogel (lyophilized) supported by a palm leaf tip, respectively.

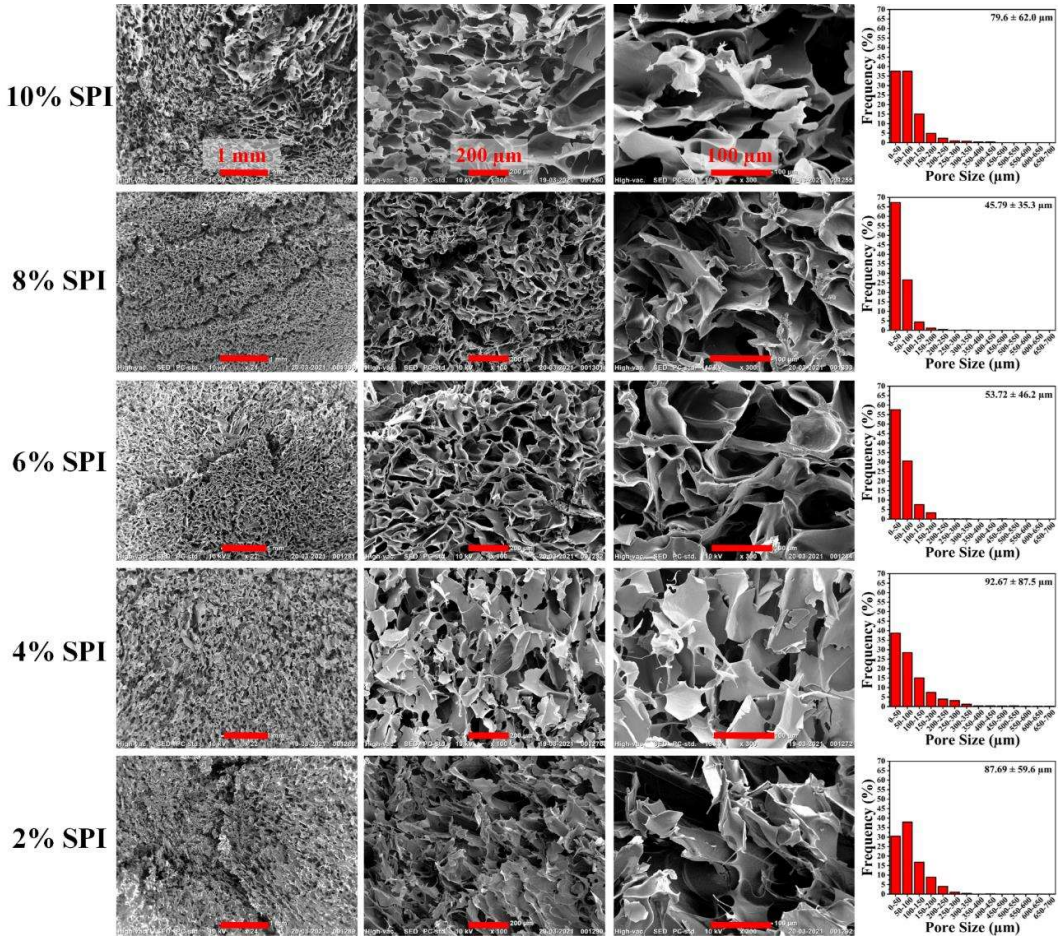

Figure 4.3 Morphological analysis through SEM photomicrographs at different magnifications of all the prepared lyophilised SPI cryogel samples of different concentrations: 10%, 8%, 6%, 4% and 2% SPI, along with their respective pore size distribution graphs.

4.3.2 Porosity of SPI cryogels

In tissue regeneration, porosity performs a crucial function. It measures the overall void space in a scaffold that is necessary for cell infiltration and neovascularization. The porous network structure facilitates the development of new tissues. The porosity was determined by comparing the total EtOH volume in the cryogel to its corresponding apparent volume. An excellent porosity was obtained in all the prepared cryogels. Moreover, the porosity of cryogels decreased with increase in the SPI concentration. The

obtained porosity values were 80.07 ± 5.6, 94.65 ± 0.6, 91.93 ± 2.78, 86.98 ± 1.54 and 79.08 ± 6.92 for 2%, 4%, 6%, 8% and 10% SPI samples, respectively (Figure 4.4).

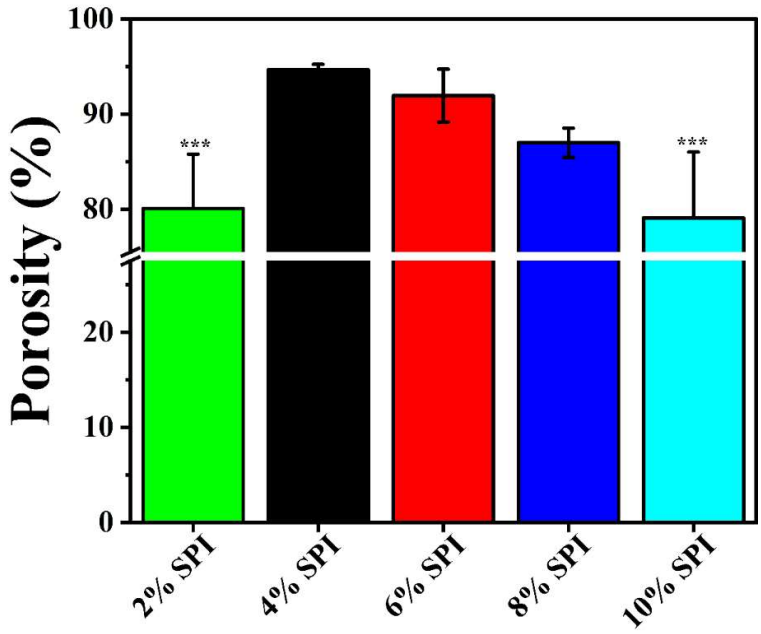

Figure 4.4 Porosity percentage of all the prepared SPI cryogel scaffolds. Values are expressed as mean ± SD (n = 3) and the level of significance as ***p < 0.05.

4.3.3 Swelling ability and water retention capacity of the prepared SPI cryogels

The swelling percentage of cryogels rose dramatically over time and reached near-equilibrium within 60 min of immersion in PBS solution. All the samples showed more than 1000 % swelling or weight gain from their initial dry weight. Among all the prepared cryogel compositions, the 4% SPI sample showed the highest swelling percentage of 2285.26 ± 671.8 %. The swelling percentage of SPI cryogels gradually decreased from 2285.26 to 1058.6% with a gradual increase of polymer content in the cryogels (Figure 4.5(a)). The maximum water content (MWC) values obtained were 92.4 ± 3.04 % for 10% SPI, 93.49 ± 4.15% for 8% SPI, 94.7 ± 5.02% for 6% SPI, 96.6 ± 2.03% for 4% SPI and 94.8 ± 4.01% for 2% samples (Figure 4.5(b)). Intuitively, the high density of micrometre-sized pores in the samples enabled absorption of large amount of liquid and

hence the samples exhibited superabsorbent properties. Both porosity (%) and pore size were found to be significantly correlated (positively) with swelling (%) and the individual correlation values are +0.9173 and +0.9926, respectively. Thus, with an increase in porosity (%) or pore size, the swelling (%) also increases as also evident from the result in the given Figure 4.6 where swelling (%) versus pore sizes and porosity (%) plots for the fabricated SPI cryogels have been plotted. This high swelling ability make them suitable candidate for wound dressing particularly for exceedingly bleeding and draining wounds.

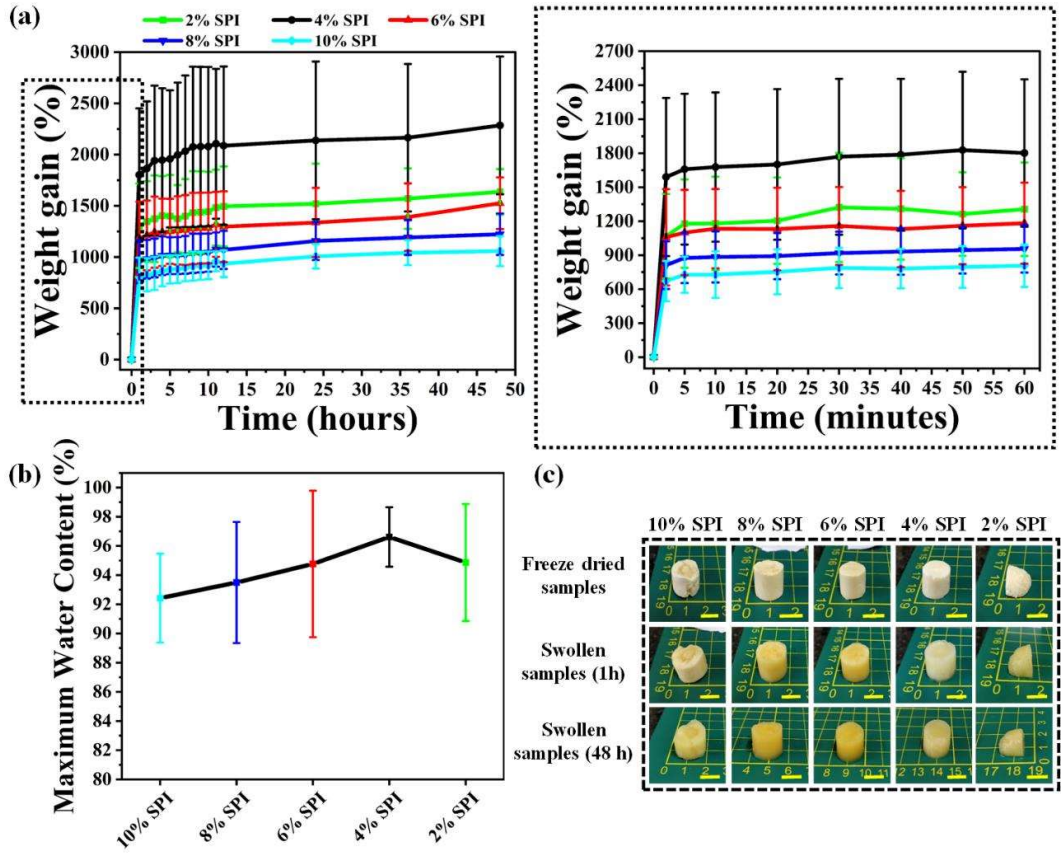

Figure 4.5 Graphs showing **(a)** weight gain percentage up to 48 h **(b)** maximum water content percentage of all the prepared lyophilised SPI cryogel samples of different concentrations: 10%, 8%, 6%, 4% and 2% SPI, in PBS at room temperature (25 °C). **(c)** Digital images of all samples: dry state (before swelling), wet state (after 1 h and 48 h of swelling in PBS). Values are expressed as mean ± SD (n = 5). Scale bar: 10 mm.

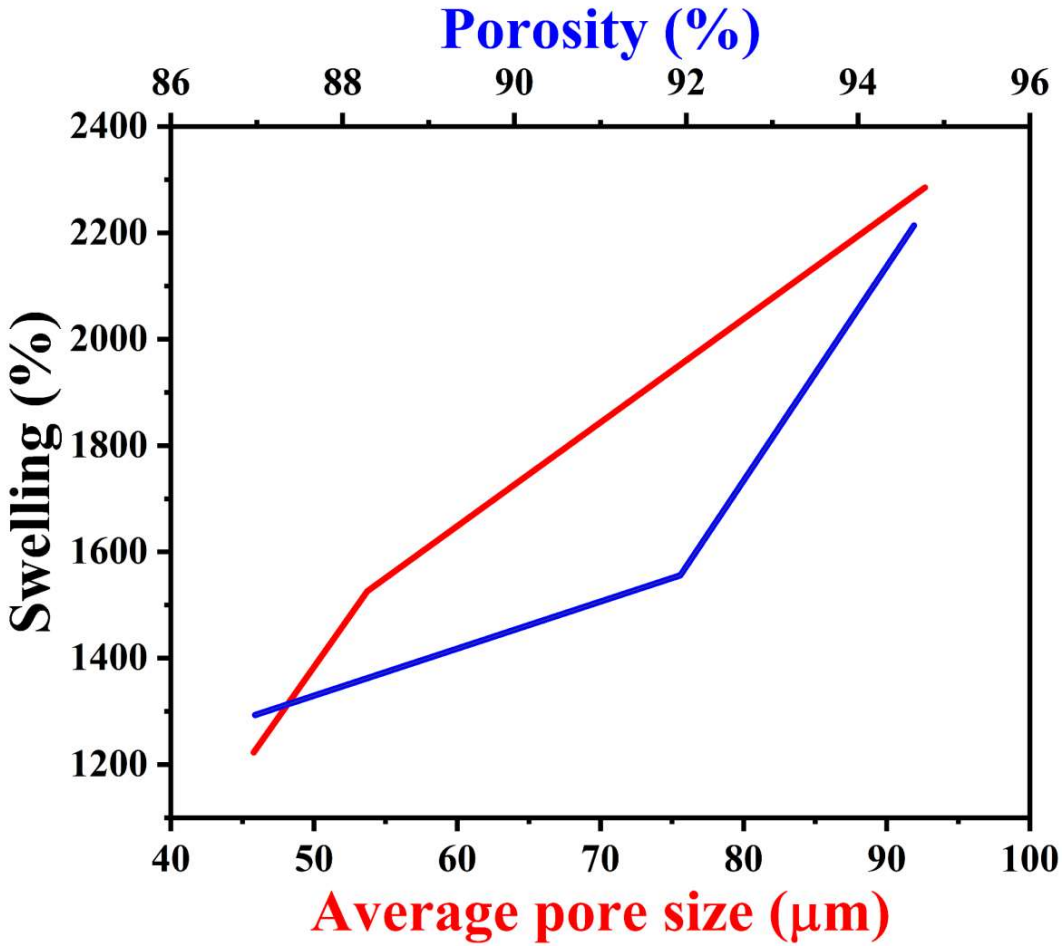

Figure 4.6 Swelling (%) versus pore sizes and porosity (%) plots for the fabricated SPI cryogels.

Even after employing multiple manual compression cycles, SPI cryogels were found to be able to recover their initial morphology after reabsorbing the water lost during compression (Figure 4.7). We observed that during compression the hydrogels released water from them and compressed to about one-fifth from their original length. After removing weight they absorb all the released surrounding water and regain their original shape. Therefore, the formed hydrogels have high elasticity, near perfect shape recovery and good mechanical strength, which is also evident from the mechanical testing results. Furthermore, it was observed that about 2 mm thick compressed hydrogel absorbs 3 mL water within few seconds. The 4% SPI hydrogel showed the maximum water absorption among all the fabricated samples. To sum up, the fabricated hydrogels rapidly absorb

plenty of water from their surrounding and hence can be useful for many applications such as wound dressing, napkins etc.

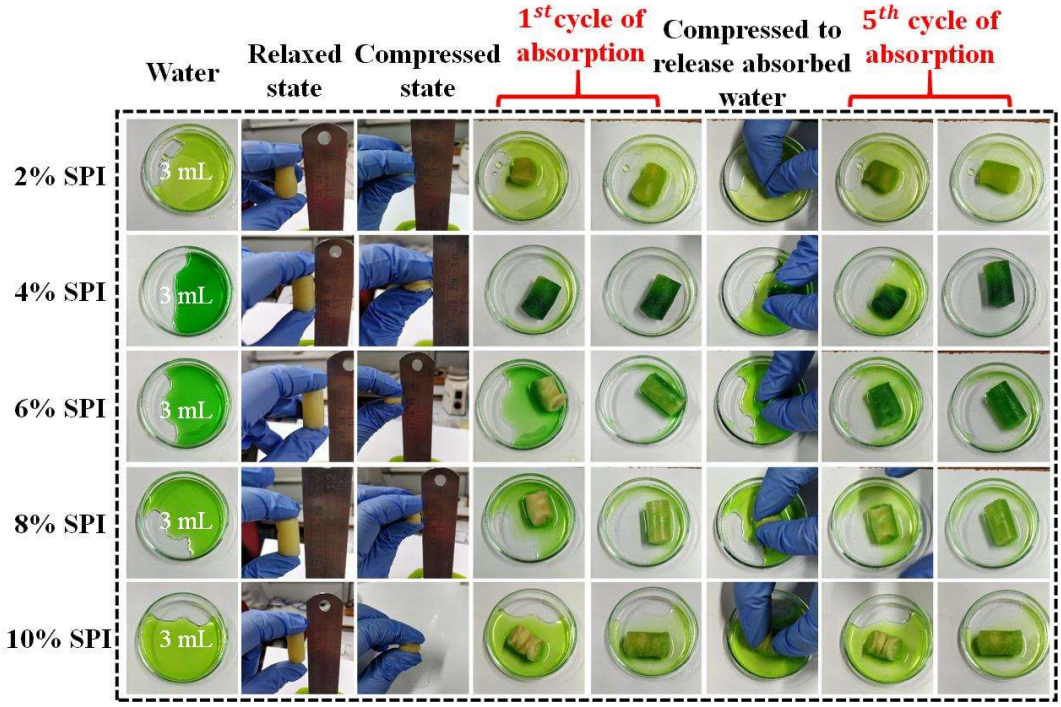

Figure 4.7 Digital images show cyclic swelling (swelling and squeezing) of SPI cryogels by performing manual compression.

The water retention capacity graphs of the samples with respect to time at 37˚C up to 48 h, showed no significant difference in rate of water loss from the samples. However, up to 10 h, the 8%, 6%, and 2% SPI cryogels exhibited slightly higher water retention than the 4% and 10% SPI samples. For instance, within 10 h, 2%, 4%, 6%, 8% and 10% SPI samples lost about 61.73 ± 13.4%, 76.05 ± 14.01%, 62.77 ± 17.5, 58.1 ± 15.6 and 79.71 ± 7.15% water, respectively. Furthermore, the rate of water loss increased with time. They lost more than 50% water within 12 h and about 90% in 48h (Figure 4.8). These findings can be attributed to the smaller pore sizes in the 8%, 6% and 2% SPI. Thus, it can be inferred that small pore size makes it difficult to lose water and hence plays an important role in water retention.

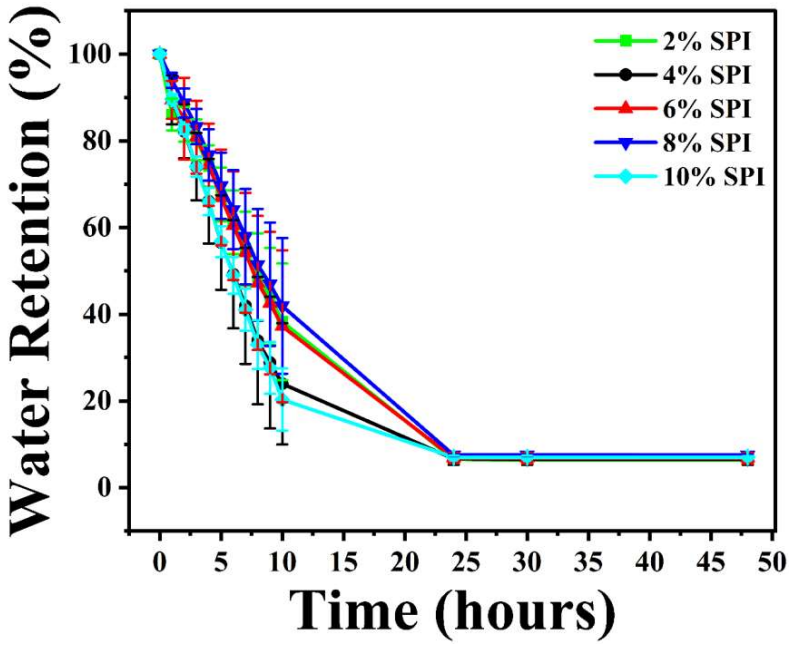

Figure 4.8 Changes of water retention rate with respect to time at 37 °C and 50% relative humidity.

4.3.4 Stability and degradation of SPI cryogels

The stability and degradability of any scaffold determine its suitability for use in various TE applications. The fabricated SPI cryogels gradually degraded after 12 days of incubation in PBS and lysozyme containing solutions. Specifically, after 12 days of incubation in PBS solution, the 2%, 4%, 6%, 8%, and 10% SPI samples were found to be degraded by 4.5 ± 0.82, 5.52 ± 1.02, 4.92 ± 0.95, 6.26 ± 0.91 and 17.9 ± 2.03%, respectively (Figure 4.9(c)). The degradation rate was found to be slightly higher in the lysozyme containing solution (Figure 4.9(d)). No discernible change in the physical appearance of examined samples was found in digital images as well as SEM micrographs (Figure 4.9(a) and (b)).

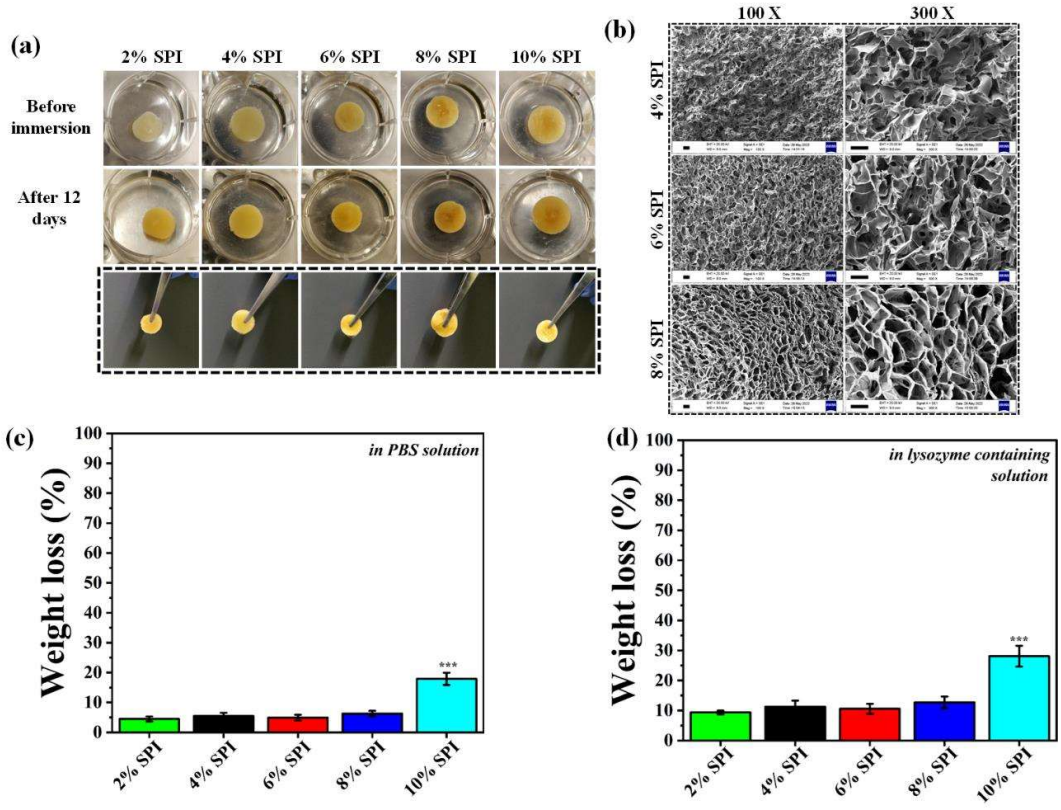

Figure 4.9 Degradation study: **(a)** digital images showing SPI cryogel samples (10%, 8%, 6%, 4% and 2% SPI) in PBS solution before and after 12 days of in vitro degradation. **(b)** SEM micrographs of lyophilized SPI cryogel samples after 12 days of in vitro degradation in PBS solution at 37 °C. Scale bar: 100 µm. **(c, d)** graphs showing weight loss percentage of all the prepared SPI cryogel samples in PBS and lysozyme-containing solution, respectively, at 37 °C. Values are expressed as mean ± SD (n = 3) and the level of significance as ***p < 0.05.

4.3.5 FTIR analysis

FTIR spectroscopy was performed to confirm the presence of functional groups and linkages in the obtained cryogels. The FTIR spectra of all the samples showed major peaks at 3276, 2963, 2918, 1631, 1518 and 1234 cm^{-1} wavenumbers representing N-H stretching vibration (amide A), asymmetric C-H vibration, symmetric C-H vibration, C=O stretching vibration (amide I), N-H bending (amide II), and C-N stretching, respectively (Figure 4.10). The C-O stretching peak (1750 cm^{-1}) and C-H stretching (~2825 cm^{-1}) of GA were not observed in all the prepared cryogels, which confirms the

absence of free GA in all samples (Patro and Wagner 2016; Mansur et al. 2008). It can be inferred that during multiple washings, all free GA residues were removed from the samples. No new peaks were observed after the crosslinking with GA. However, a slight shifting of the C-O stretching peak from 1057 cm^{-1} to 1047 cm^{-1} was observed after GA crosslinking. These results confirm the successful cross-linking of GA with SPI.

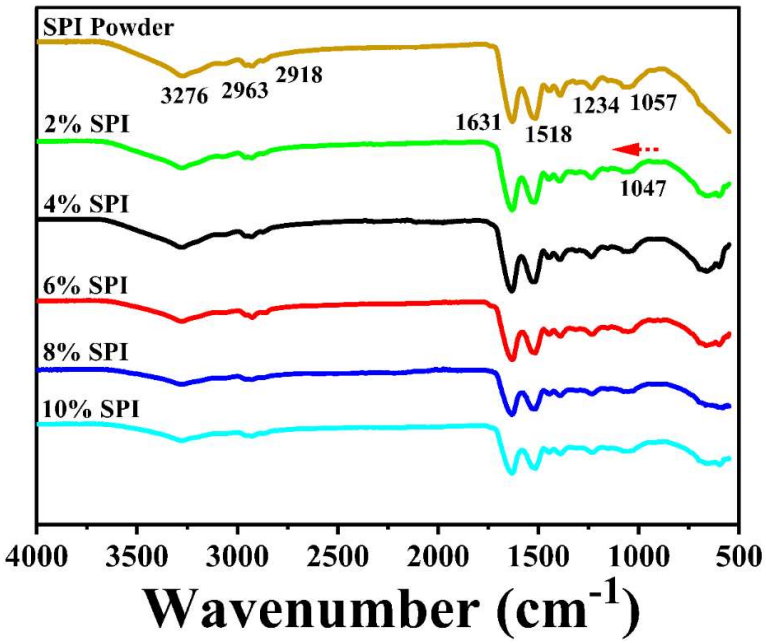

Figure 4.10 FTIR spectra of all the prepared SPI cryogel scaffolds.

4.3.6 Thermal properties of prepared SPI cryogels

The mass loss of each sample in relation to temperature was measured by thermogravimetric analysis of the lyophilized SPI cryogels. Evaporation of adsorbed and surface water from the samples caused the initial weight loss in the TGA curve to occur below 100 ºC. The second weight loss was noticed between temperatures of 180 ºC to 454 ºC and might be due to the breakdown of the polymer's main chain (Figure 4.11(a)). The degradation temperature (T_d) is the temperature at which a significant weight loss occurs, which is measured from the endothermic peak of the derivative weight (%) curve (Figure 4.11(b)). The T_d value of 312 ºC for 2% samples shifted to lower temperature that

is 292 ºC for 10% SPI samples. This might be because of the low crosslinking in 10% SPI samples. Moreover, the weight loss percentage at 500 ºC was observed to lie between 60 to 65% for all the samples.

The DSC thermogram of SPI powder revealed no T_g or T_m values. Similarly, no significant changes were observed in SPI cryogels after cross-linking with GA (Figure 4.11(c)).

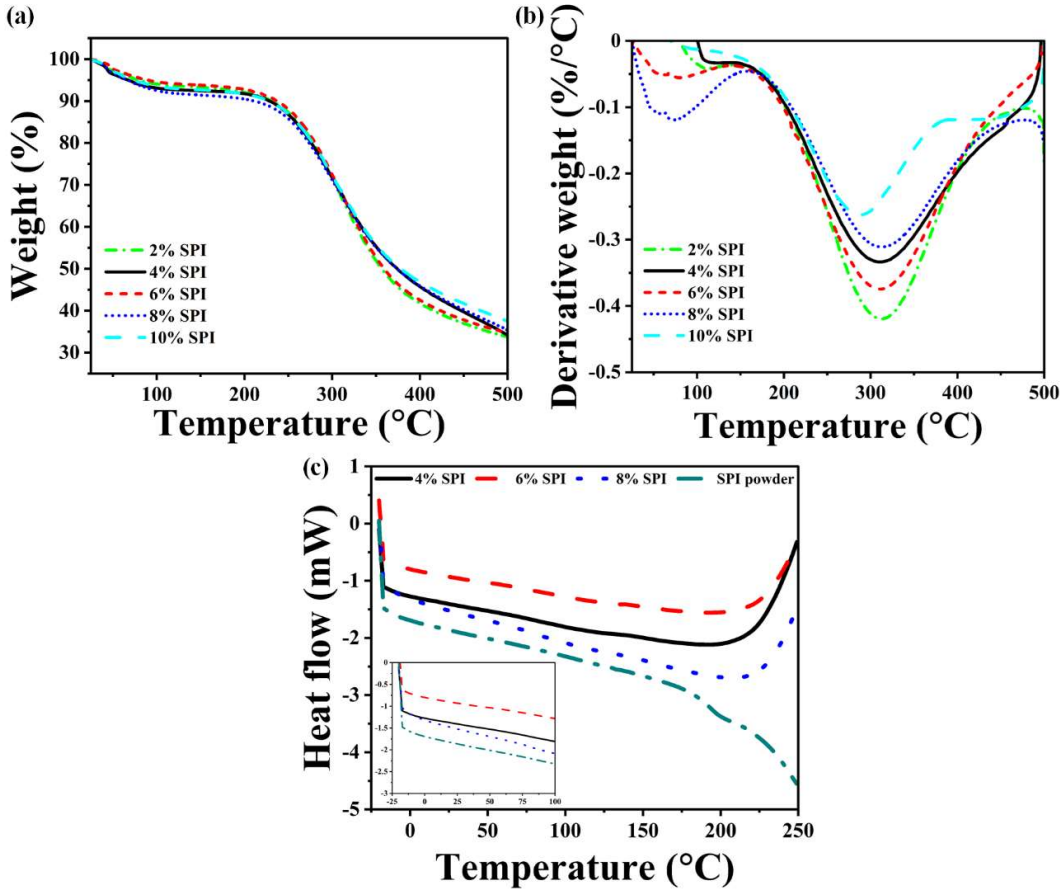

Figure 4.11 (a) TGA **(b)** DTA curves and **(c)** DSC curves of SPI powder, 4%, 6% and 8% SPI cryogels.

4.3.7 Mechanical properties

For TE applications, the synthesised scaffolds should preserve their mechanical integrity as well as provide mechanical strength to the damaged tissue. To determine the compressive properties of the fabricated cryogel samples, uniaxial stress was applied on them (Figure 4.12). The Young's modulus was calculated from the slope of the initial region of the stress vs strain curve. (Figure 4.12(b)). The compressive strength of the prepared samples was obtained using the compression test. For 50 % compression, the maximum compressive strength of 0.0306 ± 0.00302 MPa was obtained for 8% SPI samples, followed by 0.0086 ± 0.0007 MPa for 6% SPI and 0.00315 ± 0.0004 MPa 4% SPI samples (Figure 4.12 (b)). The compressive strength increased to almost twice for 8% SPI and approximately four times for 4% SPI and 6% SPI samples, at 80% compression (Table 4.2, Figure 4.12(c)). The compressive modulus values of the samples at 50% compression were found to be 0.5913 ± 0.052 kPa, 0.287 ± 0.009 kPa, and 0.085 ± 0.016 kPa for 8% SPI, 6% SPI, and 4% SPI samples respectively (Figure 4.12(d)). Compression tests for 10 cycles were also performed at both 50% and 80% compressions. The obtained results revealed that all the prepared scaffolds had a very insignificant loss in compressive strength (~5%) during multiple compression cycles (Figure 4.13 (a)-(f)). Overall, the 8% SPI sample showed the maximum compressive strength and modulus among all the fabricated scaffolds. Moreover, it can be inferred that all the cryogel samples have the ability to undergo multiple compression and relaxation cycles while maintaining their mechanical properties. Furthermore, it can be noted that the stiffness of the samples increased with the polymer concentration.

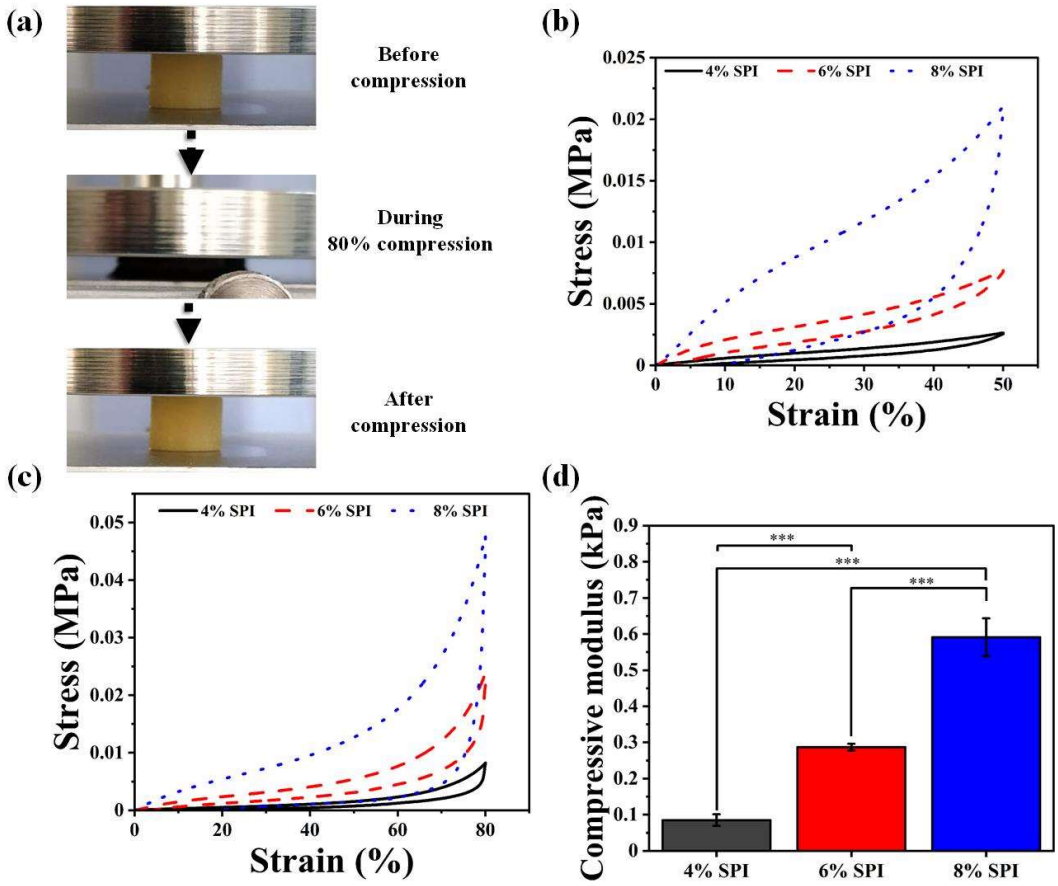

Figure 4.12 Mechanical properties of prepared SPI cryogels: **(a)** photographs of the compression behaviour of 6% SPI cryogel under instrumental control. Cycle curves were obtained immediately after one loading-unloading cycle of SPI cryogels at **(b)** 50% compression **(c)** 80% compression. **(d)** Compressive modulus values of 4%, 2% and 8% SPI cryogels.

Table 4.2: Mechanical properties of prepared SPI cryogels: Compressive strength at 50% and 80% compression, and compressive modulus.

Sample	Compressive strength at 50% compression (MPa)	Compressive strength at 80% compression (MPa)	Compressive modulus (kPa)
4% SPI	0.00315 ± 0.0004	0.01205 ± 0.00225	0.085 ± 0.016
6% SPI	0.0086 ± 0.0007	0.03421 ± 0.00312	0.287 ± 0.009
8% SPI	0.0306 ± 0.00302	0.05097 ± 0.00221	0.5913 ± 0.052

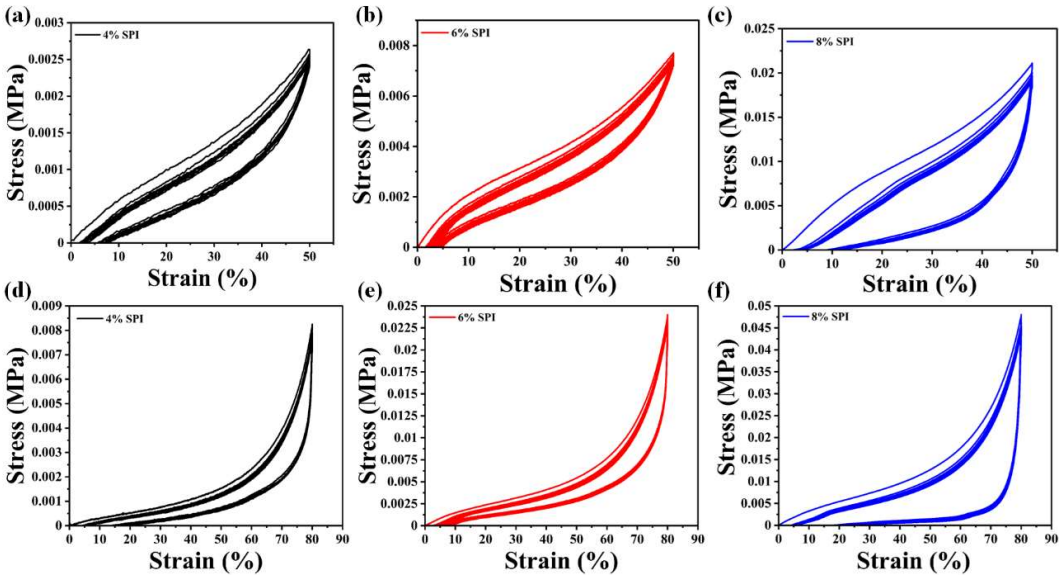

Figure 4.13 Compressive stress-strain curves at 50% strain under 10 loading-unloading cycles of **(a)** 4% SPI, **(b)** 6% SPI and **(c)** 8% SPI cryogel samples. Compressive stress-strain curves at 80% strain under 10 loading-unloading cycles of **(d)** 4% SPI, **(e)** 6% SPI and **(f)** 8% SPI cryogel samples.

Dissipation energy is a common property of viscoelastic materials like polymeric scaffolds. It corresponds to the energy absorbed by the hydrogel network from an incoming impact. The stress-strain graph (Figure 4.13) shows a hysteresis loop because the scaffold dissipated energy in the course of the cyclic compression testing. The area under the hysteresis loop represents the dissipation energy or the mechanical energy that has been lost (Chen et al. 2016). Single loading/unloading cycle was performed at 50% and 80% compressions for 4%, 6%, and 8% hydrogels. The maximum dissipating energy of 6.783 KJ/m^3 and 12.553 KJ/m^3 was observed at 50% and 80% compressions, respectively, for 8% SPI samples. The hydrogels with 4% SPI and 6% SPI, showed the dissipating energy of 0.987 and 3.189 KJ/m^3, respectively at 50% compression, whereas at 80% compression, 2.11 KJ/m^3 and 7.376 KJ/m^3 dissipation energy values were observed. The variation in the dissipating energy indicates that the stretchability and mechanical strength can be optimized for hydrogels by changing the concentration of SPI.

The maximum dissipation energy of 8% SPI indicates comparatively high mechanical properties of the sample suggesting that the sample has a potential to dissipate large amount of incoming force acting on the optimized concentration for making mechanically stable hydrogels. By comparing the dissipation energy of different scaffolds, more application specific material selection can be ensured for tissue implants. Abdel-Sayed P. et al. found that the scaffolds with higher dissipation energy were associated with upregulation of the chondrogenic markers' gene expression whereas the scaffolds with less dissipation energy downregulated the chondrogenic markers. They also showed that the dissipation level was higher in scaffolds with higher cross-linking density compared to scaffolds with less crosslinking under an identical dynamic compression test (Abdel-Sayed et al. 2014). Overall, the increase in SPI content in cryogel significantly increased the elastic modulus or stiffness and dissipation energy of the scaffolds. Therefore, from the above discussion it can be concluded that energy dissipation could be considered as one of the key mechanobiological factors in tissue engineering.

Cryogelation process produces shape-memory elastic SPI cryogels (Figure 4.14). The shape volumetric expansion ratio, fixity ratio, and recovery ratio values of SPI cryogels are presented in Table 4.3. The SPI cryogels showed a decrease in their volumetric expansion ratio (V_E) with the increase in SPI content. Furthermore, fixity ratio (R_f) was also found to decrease from 95 ± 0.4 to 77.7 ± 1.5% with an increase in SPI content from 4% to 8%. In less than 20 seconds, all the samples regained their initial shape (with a recovery ratio of 100%) after getting in contact with water.

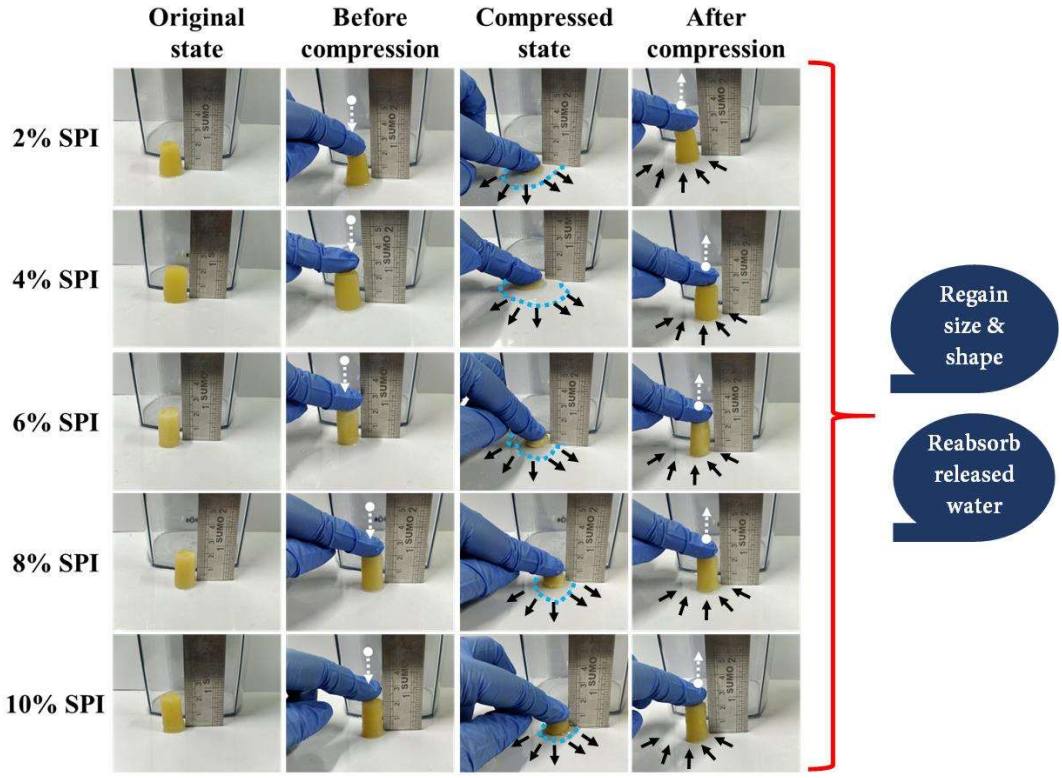

Figure 4.14 Shape recovery properties of the cryogel: original state in a wet condition, before compression, compressed state (fixed shape) after releasing all free water, after compression recovered shape by reabsorbing the released water.

Table 4.3: Shape fixity ratio, recovery ratio and volumetric expansion ratio of the water-triggered shape recovery process of the SPI cryogels.

Sample	R_f (%)	R_r (%)	V_E
4% SPI	95 ± 0.4	100	5.6 ± 0.4
6% SPI	81.81 ± 0.7	100	3.7 ± 0.2
8% SPI	77.77 ± 1.5	100	1.6 ± 0.2
R_f : Strain fixity ratio; R_r: Strain recovery ratio; V_E: volumetric expansion ratio			

4.3.8 Hemocompatibility of SPI cryogels

Hemocompability is one of the most important criteria for selecting the blood-contacting biomaterials for in vivo applications. The in vitro hemolysis assay is the most commonly used method for determining a material's hemocompatibility (Zhao et al. 2018). Figure 4.15 (a) shows the macroscopically colour of supernatants obtained after centrifugation of all cryogel groups, the negative group (PBS), and the positive group (distilled water). The positive group appeared to be red in colour, whereas, similar to the negative control group, the other three cryogel groups were nearly transparent. The absorbance values obtained from the hemolysis test were 0.0443 ± 0.0015, 0.045 ± 0.001, 0.048 ± 0.002, 0.0443 ± 0.0013 and 0.6533 ± 0.0037, for the samples exposed to 4% SPI, 6% SPI, 8% SPI, the negative control, and the positive control, respectively. In the presence of 4% SPI, 6% SPI and 8% SPI samples, the degree of hemolysis was 0.0547 ± 0.2508, 0.1094 ± 0.1896 and 0.6568 ± 0.3284%, respectively (Figure 4.15 (b)). In general, a useful biomaterial should have a hemolysis rate of less than 2%. A higher degree of hemolysis implies that the biomaterial is not hemocompatible. The obtained results suggest that SPI cryogel samples provide an adequate level of hemolysis.

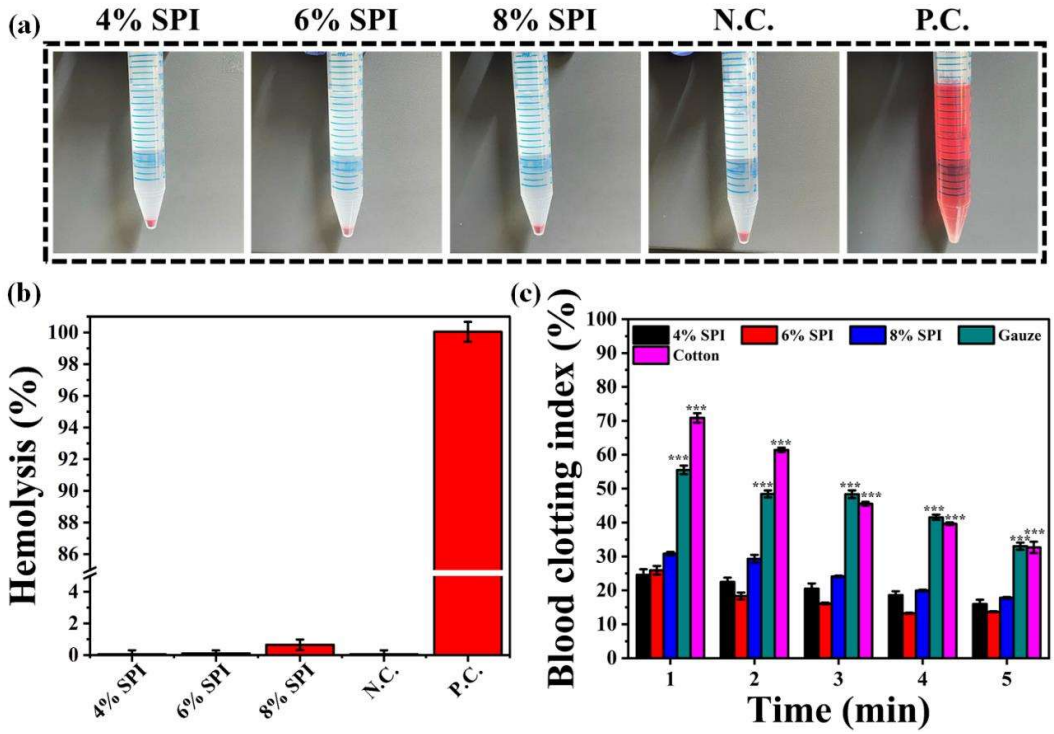

Figure 4.15 (a) Images from haemolytic activity assay of the SPI cryogels using PBS as negative control (N.C.) and distilled water as positive control (P.C.). **(b)** Haemolytic percentage of the SPI cryogels' dispersion liquids. In vitro hemostatic capacity evaluation of SPI cryogels **(c)** in vitro whole blood clotting evaluation of cryogels and controls (gauze and cotton).

4.3.9 In vitro blood clotting performance of SPI cryogels

The cryogels' blood clotting capacity was assessed using the dynamic whole-blood clotting test, wherein a higher haemoglobin solution absorbance value signifies a slower clotting rate. Intuitively, lower is the percentage of erythrocytes entrapped by clots, higher is the percentage of free erythrocytes and in turn higher is the absorbance of haemoglobin in the water. Thus, absorbance is inversely proportional to the clotting rate or clot size. Conventional hemostatic agent i.e. gauze and cotton were considered as control groups. In comparison to control groups, all the tested cryogel samples showed quicker absorption of blood. Moreover, the obtained BCI of prepared SPI cryogels (4%, 6% and 8%) was significantly lower than that of the control groups at each time point (Figure 4.15 (c)).

The hemostatic mechanism was examined further by studying the morphologies and surface adherence of blood cells on SPI cryogels, as well as on gauze and cotton (control groups) (Figure 4.16). In terms of blood cell adherence, all the cryogels were found to be densely packed with blood cells, whereas significantly lesser number of blood cells were found on the surface of the two control groups. In all three SPI cryogels, a significant amount of blood cells adhered to the pore surfaces and aggregated together. Overall, these findings show that SPI cryogels can effectively clot the blood. This is possibly due to the high porosity and composition of the fabricated cryogel samples.

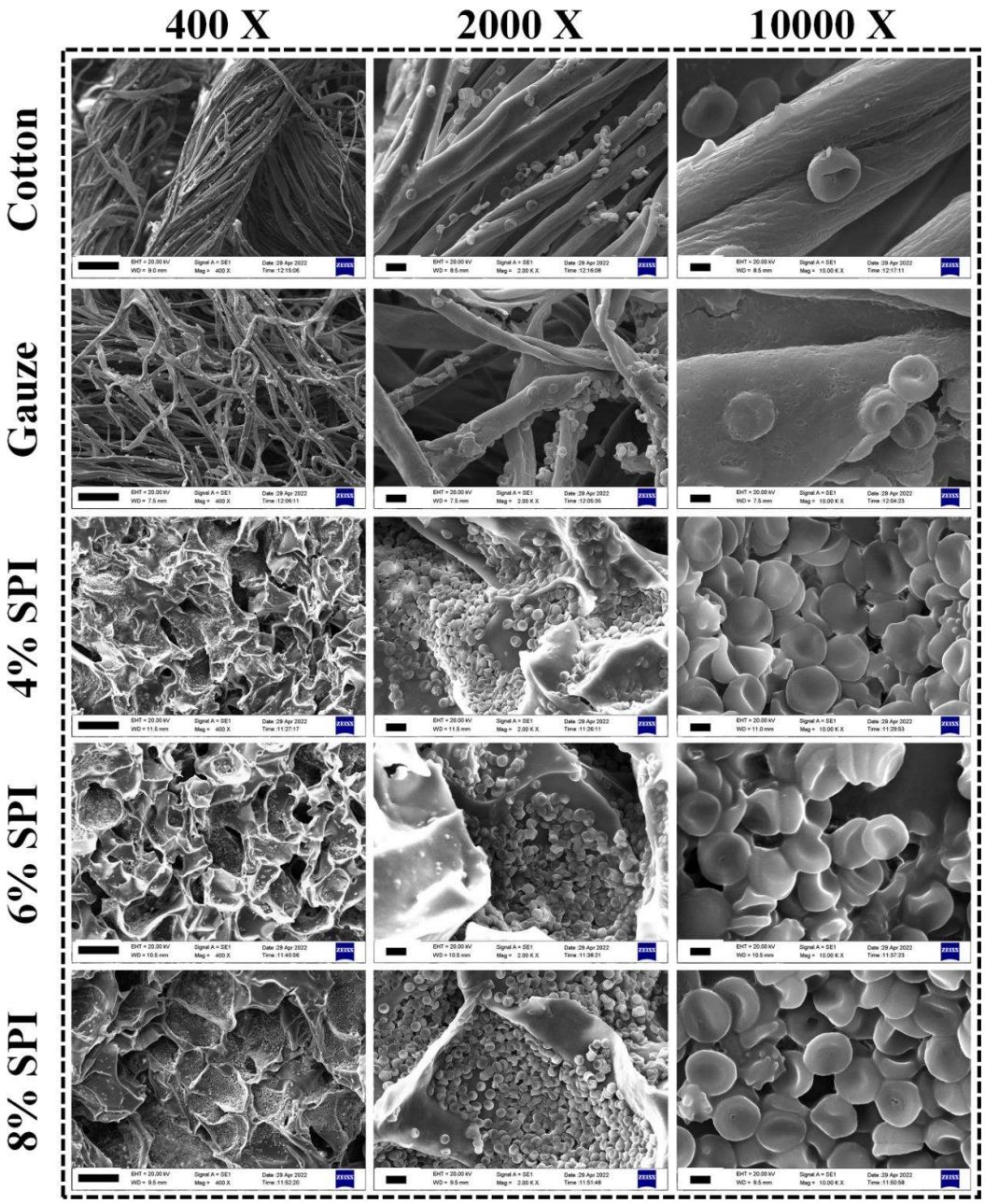

Figure 4.16 SEM images of blood cells adhesion on the SPI cryogels and controls (gauze and cotton). Scale bar: 100 µm for 400X; 10 µm for 2000X; 2 µm for 10000X.

4.3.10 Cellular biocompatibility of prepared SPI cryogels

To study the suitability of cryogels toward mammalian cells, L929 cells (fibroblast) were cultured with in the sterilized hydrogels and analysed through fluorescent microscopic

images up to 10 days. From the in vitro cell culture images, quite high cell density and good interconnectivity were observed between the cells in all the samples. Blue coloured nuclei within the samples were clearly visible in the DAPI stained images at high magnification (Figure 4.17). Cell density was found to be increasing with time.

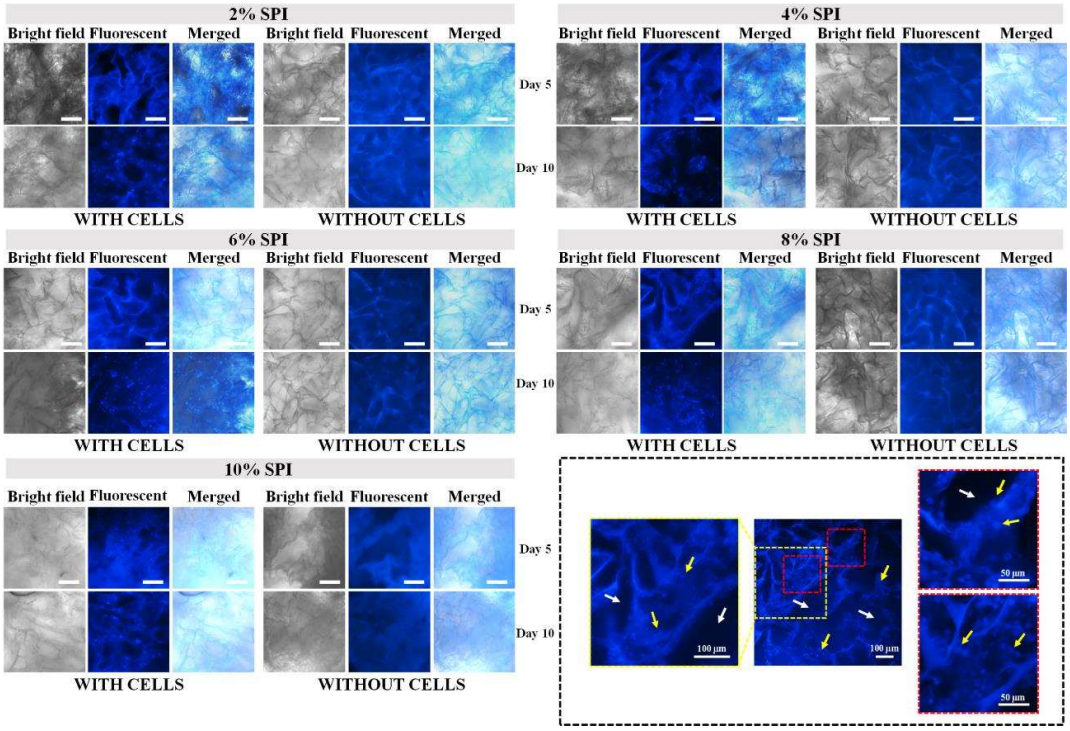

Figure 4.17 The above panel of microscopic images represents the culture of L929 (fibroblast) cells within the SPI cryogels for over a period of 10 days. Cryogels without cells were taken as control. Scale bar: 100 µm for bright-field, fluorescence, and merged images. The fluorescence images in the dotted rectangle are at different magnifications to clearly visualize the nucleus (DAPI staining) of the cultured cells within the SPI cryogels.

Furthermore, SEM images of the L929 cell-cultured SPI cryogels showed remarkably good cell adherence, growth, and proliferation (Figure 4.18). For up to 12 days of cell culture, no substantial physical breakdown of SPI cryogels was observed.

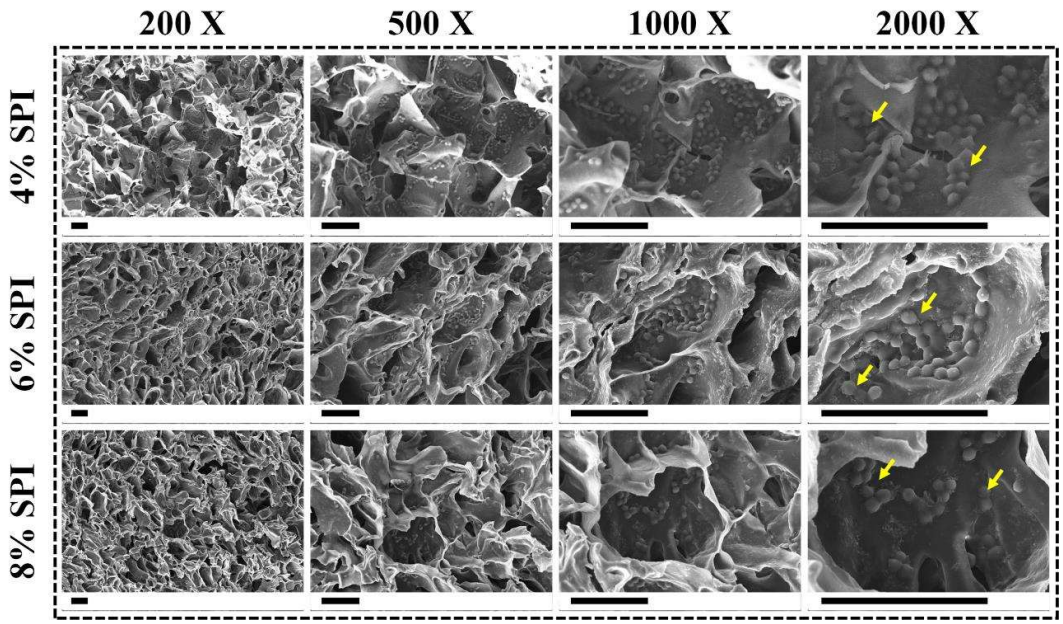

Figure 4.18 SEM images of L929 (fibroblast) cells cultured on SPI cryogels: 4%, 6% and 8% SPI cryogels. Scale bar: 100 μm.

For quantitative analysis, the cellular viability percentage of cells and the biocompatibility of the prepared hydrogels were determined by MTT assay. From the results of MTT assay, the cellular viability in cryogel samples was found to be significantly higher than that in control. The 4% SPI samples showed about 120% cell proliferation which is significantly greater than that in control (Figure 4.19). Overall, these results reveal that soy protein cryogels promote cell infiltration, attachment, growth and proliferation.

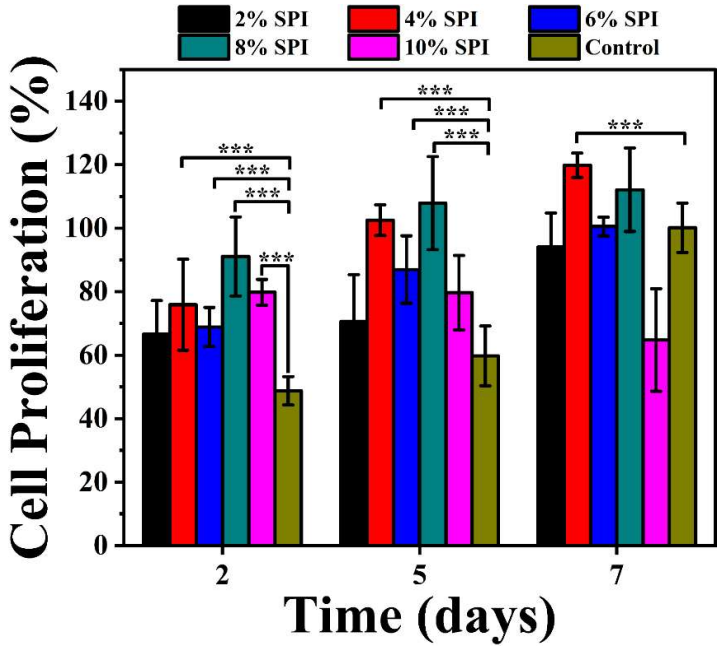

Figure 4.19 Percentage cellular viability of L929 (fibroblast) cells and the compatibility of the SPI cryogels determined by the MTT assay. In the MTT assay experiment, the absorbance for the 7^{th} day culture of positive control (cultured cells without cryogel samples) was taken as the reference OD for all the samples. Values are expressed as mean ± SD (n = 3) and the level of significance as ***$p < 0.05$.

4.3.11 In vivo wound healing

We have examined the applicability of the fabricated SPI cryogels as a wound dressing for skin tissue regeneration. We studied the wound healing process of a full-thickness wound that had been excised in rat models for up to 16 days. The rats were divided into three groups: 1st sham- without any treatment, 2nd treated with 4% SPI samples, 3rd is treated with 6% SPI samples. Each group contained 3 rats (n = 3). It was observed that both 4% and 6% samples got adhered excellently on wound bed (Figure 4.20(b)). Over the course of time, each of the cryogel samples deteriorated gradually. On day 10, sample treated groups attained more than 80% wound closure, whereas sham group acquired closure up to 65% only. On day 14, sample treated groups attained almost 100% wound closure whereas sham group obtained approximately 90% closure of wound (Figure

4.20(c)). The protein content and the interconnected porous nature of the cryogel samples might be the explanation behind accelerated wound healing in sample-treated groups. No significant difference was observed between the healing rates of both type of samples treated groups. Intuitively, the wound healing rate in the sample treated groups got enhanced during the degradation of samples due to the exposure of the adhesive moieties and peptides present in the soy protein to the wound. No unfavorable effects such as fluid confinement, infection, granulation tissue bleeding, sepsis, animal death etc. were observed during the whole experiment. For histological studies, the animal were sacrificed after the 16^{th} day and variations in the healed tissues were subsequently examined using H&E staining. Figure 4.20 (d) shows the H&E staining images of sham, 4% SPI and 6% SPI treated groups. 4% SPI and 6% SPI cryogel treated groups exhibited complete re-epithelization and thicker epidermis layer compared to the sham group. The presence of keratinocyte cells in the epidermal layer and the deposition of collagen in the dermal layer indicated that the wound healing process had been completed. The sham group presented reduced re-epithelization compared to the treated groups. Furthermore, in addition to improved reepithelialisation, we noticed the existence of dermal appendages, including hair follicles and sweat glands, in healed skin tissue after the treatment with SPI cryogel matrices. From all these outcomes, it can be concluded that SPI cryogels promoted wound healing by dual effect of cell matrix interactions and excess exudate absorption, which may also take part in homeostasis acceleration.

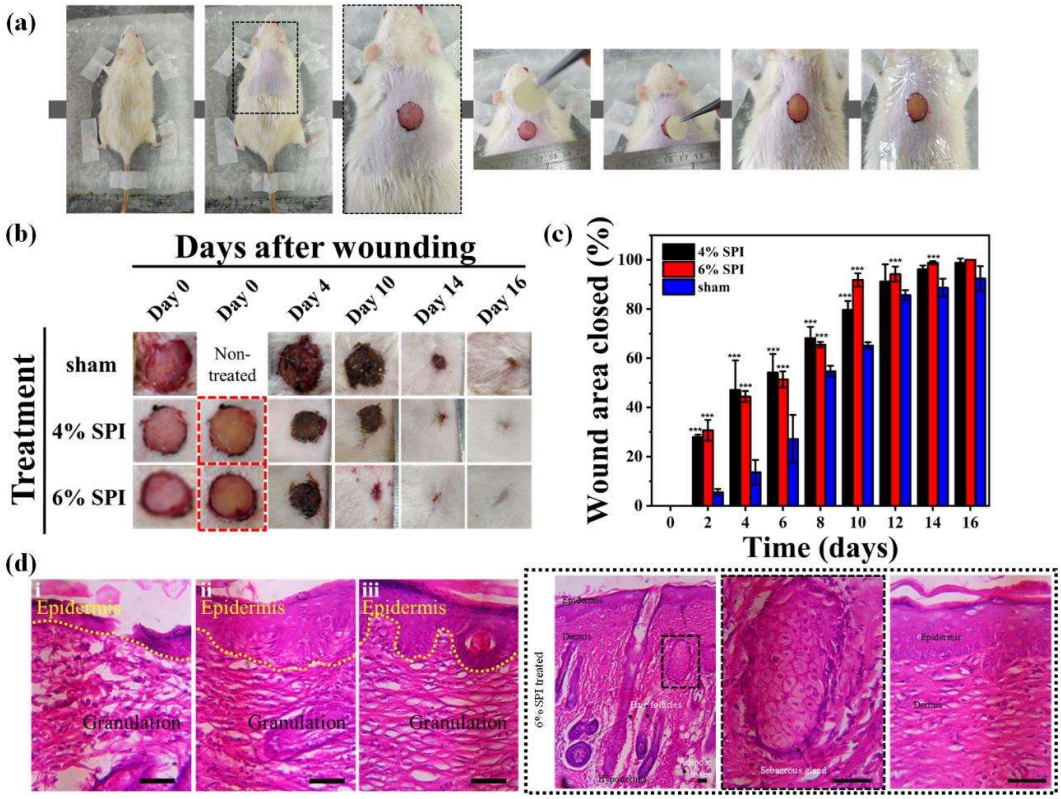

Figure 4.20 Figure showing in vivo wound healing: **(a)** digital photographs of full thickness excision wound and application of SPI cryogel to the wound **(b)** digital photographs of full thickness wound closure on days 0, 4, 10, 14, and 16. **(c)** Graph depicting a comparison of wound area closed percentage of cryogel treated and sham (untreated) groups **(d)** micrographs of H&E stained tissues: (i) sham group, (ii) 4% SPI treated, (iii) 6% SPI treated skin tissues; higher magnifications images of histological sections (H&E stains) of 6% SPI treated skin tissues in dotted rectangle. In cryogel treated wounds, the connective tissue is found to be more organized and developed than the untreated wounds. Values are expressed as mean ± SD (n = 3) and the level of significance as ***$p < 0.05$. Scale bar: 50 μm.

4.4 Discussion

We fabricated superporous cryogels (hydrogels) at sub-zero temperatures by the process of cryogelation, which involves the polymerization of polymeric precursors or monomers. First, the monomeric or polymeric precursors were dissolved in a solvent, like deionized water, and then cross-linker was added. The entire combination was then immediately incubated under freezing conditions. The solvent froze during the creation of cryogels at sub-zero temperatures, resulting in the development of ice crystals (which act as

porogen). These ice crystals continued to expand and linked with one another. Some solvent or solute molecules in the solution were not completely frozen (known as the unfrozen liquid microphase). It is important to note that SPI and GA concentrations rise dramatically in liquid microphase volume, and this process of solute enrichment is called the cryo-concentration effect. This occurs because as the solvent crystallizes, the concentration of solutes increases due to their ejection into the volume of liquid microphase. These concentrated solute precursors polymerize and crosslink in the liquid microphase, resulting in the creation of polymeric reactions and a cross-linked gel like structure (cryogel) (He et al. 2021). Interestingly, such cryo-concentration effects not only entirely overcome the unfavourable effects of low temperature, but also significantly lowers the critical concentration of gelation of the polymer and cross-linker (precursors), with respect to that observed for the gelation in the same initial systems at positive temperatures. As a result of these cryo-concentration effects, the rate of chemical reactions and intermolecular interactions in unfrozen inclusions, which operate as microreactors, is significantly accelerated (Lozinsky 2002). Here, we found that cryogels could be produced at a substantially low concentration of polymer as well as cross-linker at -12 °C for 24 h; however we were unable to produce bulk gels of the same concentrations at room temperature or temperatures higher than 0 °C for 24 h or longer period of time. A similar observation was reported by Mu et al. where they showed that cryogels were formed when collagen/dialdehyde starch (DAS) solutions were stored at 15 °C for 72 hours. However, no bulk gels were produced when the same solution was stored at 4 °C for 3 days or longer. (Mu et al. 2010)

The pore interconnectivity in scaffolds plays a major role in their performance, particularly for cell mobility for tissue regeneration, mass flow, and the development of bioreactors, amongst other things (Tripathi and Melo 2019). SEM analysis of lyophilized

cryogels revealed microporous mesh-like topologies with pores that were interconnected to each other. Moreover, these structures are accountable for rapid water movement, which is evident from the findings of the swelling research, in which all SPI cryogel samples had good swelling capabilities. These results show that the porous structure and SPI cause samples to swell well, which is one of the most important prerequisites for wound dressings to be able to soak up excess wound fluid. This is most likely the result of the interconnected porosity structure as well as the fact that charged amino acids, such as aspartic acid and glutamic acid, are present in SPI in relatively large quantities in comparison to hydrophobic amino acids, such as leucine. It has been shown that a moist environment significantly accelerates the rate of healing in comparison to a dry environment (Kim et al. 2008; Jones, Grey, and Harding 2006; Winter 1962). The MWC values for the prepared SPI cryogels were found to be in the range of 92 to 96%, which is significantly higher than the natural water content of normal stratum corneum which ranges from 15 to 30% of dry tissue weight (Wong, Ashton, and Dodou 2015; Silva et al. 2007). As a result of their high water content, the SPI cryogels could also be employed as transdermal drug delivery patches, as water can act as a natural penetration facilitator via hydration and high humidity. Hydration inhibits moisture loss from the skin tissue, which can affect the water level of the stratum corneum, allowing drug molecules to easily diffuse into the skin (Winter 1962; Wong, Ashton, and Dodou 2015).

We were able to achieve an average pore size of 45–92 μm, which is suitable for cell attachment, long-term cell growth, and proliferation. The obtained results demonstrate that the lyophilisation process deforms the porous structure of 2% SPI cryogel, resulting in a considerable reduction in porosity. It could be because the low polymer content makes the walls of the pores very thin. This makes the material too soft and unable to keep its shape. Moreover, we observed a reduction in the pore size and porosity of

produced SPI cryogels with increase in the SPI content. Therefore, the porosity and pore size of SPI cryogel can be adjusted by varying the concentration of SPI. Vlierberghe et al. studied the influence of polymer content on gelatin cryogel pore size. In their work, they have reported that increasing the polymer concentration leads to a reduction in porosity and pore size (Van Vlierberghe et al. 2007).

Mechanical integrity is an important aspect of TE during scaffold preparation (Sharma et al. 2013). The mechanical strength of SPI cryogels was evaluated through compression analysis. The stress was found to increase with the applied strain from 50% to 80%, and it was observed that 4%, 6%, and 8% SPI cryogels returned to their original state following unloading. The prepared SPI cryogels could be compressed to one-fifth of their original length without any irreversible distortion or fracture formation. The obtained SPI cryogels were porous, elastic, and mechanically strong in nature. Furthermore, they did not get distorted when an external pressure was applied to them or when all of the solvent that was contained within the swelled cryogel was squeezed out. This is because these produced SPI cryogels are spongy and can return to their previous shape after being submerged in water or an aqueous medium again. The polymer concentration had a significant impact on the mechanical strength of produced cryogels, since, compressive modulus and maximum compressive strength of the cryogel increased dramatically as the SPI concentration increased. Kirsebom et al. have reported that the mechanical characteristics of transglutaminase-catalyzed gelatin and casein cryogels get significantly affected by protein concentration. They observed that the increment in polymer concentration of gelatin and casein cryogels led to an increase in mechanical strength (Savina, Zoughaib, and Yergeshov 2021). In the instance of a cross-linking reaction taking place during the creation of SPI cryogel using GA as a cross-linker, the amino groups present in SPI may crosslink with the aldehyde group of GA, resulting in the

synthesis of imine. These potential bond forms were validated by FTIR, which demonstrated the presence of peaks at various wavenumbers which can correspond to functional groups and certain linkages. It has been reported that commonly used aldehydes, like formaldehyde, react with the primary amino groups and sulfhydryl groups in proteins, forming cross-links between the molecules (Curt, Subirade, and Rouabhia 2009).

3D scaffolds are used as tissue substitutes in TE. Thus, after implantation, the scaffold should degrade at a rate that is approximately equal to the rate at which the body's own tissue regenerates (Sharma et al. 2013). Overall, the rate of degradation of cryogel samples was modest in PBS solution, but under in vivo environment, this rate got accelerated owing to the presence of several enzymes and factors. Similar observation has been reported by Har-el et al. wherein they have demonstrated that soy-based scaffolds are highly susceptible to enzymatic (proteolytic) degradation in vitro and that after subcutaneous implantation, the scaffolds get rapidly degraded and completely absorbed in about 14 days (Har-el et al. 2014). Thermal stability is a key feature for end-use product applications; the SPI cryogels exhibited no noticeable weight loss in between room temperature and 150 ˚C. From this finding it can be inferred that the prepared cryogels may be sterilized in an autoclave (121 ˚C), which is critical for biomaterials.

The emergence of biomaterials having adequate hemocompatibility not only improves the tolerability but also reduces the undesirable side effects including thrombus formation in the body. As a result, not only mechanical and chemical properties, but also hemocompatibility, should be considered while developing novel blood-contacting medical implants (Weber et al. 2018). Materials can be classified into three groups based on hemolysis: materials with more than 5% hemolysis are categorised as hemolytic, those

between 5% and 2% hemolysis as moderately hemolytic, and those with less than 2% hemolysis as nonhemolytic (Totea et al. 2014). All the fabricated SPI cryogels (4%, 6% and 8% SPI) were found to be nonhemolytic. Furthermore, they all possessed an interconnected porous architecture with a high expansion ratio, which enabled them to absorb a significant volume of blood with a high swelling capacity, blood-concentrating effects, and a good absorption ability for blood cells. These characteristics all contributed to the cryogels' adequate in vitro blood-clotting outcome. The good hemocompatibility of SPI cryogels as a hemostatic agent and wound dressing was evidenced by the obtained hemocompatibility results of Figure 4.15.

The exceptional quality of being able to absorb large amounts of water in a short amount of time can make SPI cryogel a good candidate as a wound dressing. This is because it can easily absorb the excess exudate from the wound area, thereby creating a moist environment that helps lower the infection risk, and enhance the process of wound healing. In addition to allowing cells to move within the scaffold, the microporous architecture can also provide high oxygen permeability while simultaneously protecting the wound from further damage.

The biocompatibility of a scaffold is one of the most crucial requirements for TE applications (Tripathi, Kathuria, and Kumar 2009). Biocompatibility of the SPI cryogels is depicted by the obtained cell proliferation experimental results. Upon seeding L929 cells on SPI cryogels, the cells adhered and proliferated, as evidenced by fluorescent and SEM images. The findings also showed that using GA as a cross-linker had no detrimental effect on cell growth. The cell proliferation and metabolic activity of the L929 cells with in the SPI scaffold were validated by MTT assay. A significant difference in the cell proliferation was observed on 2-D surface (96-well plate) as compared to the prepared 3D SPI cryogel scaffolds. Large and interconnected pores were found in the

prepared scaffolds, which can facilitate the nutrient transport, waste and gaseous exchange. These matrices had pores in micrometre range, allowing for effective cell movement and ECM deposition. Additionally, these large and interconnected pores also facilitate the movement of nutrient medium, lowering the chances of cell death when seeding densely. Furthermore, all cryogel matrices exhibited a high pore volume, inferring that cells can easily attach to pore walls and proliferate by producing significant amounts of ECM. These matrices' high porosity enables for effective gaseous exchange, which supports cellular proliferation even in the sample's deeper regions. These properties positively impact the cell migration, growth and proliferation on these samples. Each of these attributes support the use of SPI cryogel matrices in TE.

In the context of in vivo wound healing study in rat model, the favourable benefits of the SPI cryogel scaffolds manifested in terms of the quality of wound healing. It has been hypothesized that degradation products of soy-based materials contain cryptic peptides that play a crucial function in accelerating wound healing (Har-el et al. 2014). The above findings are consistent with previous research works validating the good biocompatibility and promoted cell attachment, growth, and proliferation of the SPI-based materials. Luo et al. observed higher growth and proliferation of L929 fibroblast cells when they were grown on cellulose/SPI scaffolds than on cellulose scaffolds alone. This result was attributed to SPI hydrolysis in the nutrient medium, which made the scaffolds more porous for cell ingrowth while also delivering nutrients as degraded products of SPI during incubation (Luo et al. 2010). Lee et al. showed that the supply of low concentration of soy protein hydrolysates in culture serve as a nutrient source for human-derived epidermal keratinocyte cells and also found that the cell proliferation increased by about 200% (Lee et al. 2008). Har-el et al. demonstrated the potential of nanofibrous soy-based scaffold (SPS) as a wound dressing for the full-thickness excisional wound in

a pig model. The findings of this study indicate that SPSs have the ability to enhance re-epithelialization and wound healing processes in a more natural way that resembled the mature tissue (Har-el et al. 2014). Huang et al. prepared a tannin-functionalized SPI-based adhesive hydrogel as a wound dressing. In an in vivo study, they showed that their SPI-based hydrogel enhanced skin wound healing rate (Huang et al. 2022). Khabbaz et al. synthesized GA-crosslinked PVA and SPI nanofibrous mats and films for wound healing. They suggested, based on an in vitro cell culture investigation, that the soy-based materials possess great potential for use as wound dressings (Khabbaz, Solouk, and Mirzadeh 2019). Moreover, the inflammatory reaction of the wound tissue caused by dressing materials is known to alter re-epithelialization at the wound site. As a result, scar formation might get decreased if the inflammatory reaction could be inhibited, particularly at an early stage. In this context, soy phytoestrogens such as genistein and daidzein have been shown to promote wound healing, particularly during the inflammation period (Regal et al. 2000; E. Park et al. 2011), by reducing the activity of immune cells such as lymphocytes, monocytes, and macrophages through antioxidant and anti-inflammatory activities (Santin et al. 2007). SPI and its peptides have also been proven to improve wound healing by stimulating collagen deposition (Zhang et al. 2020). Hence, the developed SPI cryogel scaffolds in this work exhibit tremendous potential and significance as bioengineered implants for soft tissues.

4.5. Summary

SPI cryogels were successfully prepared using cryogelation technique. The average pore sizes were obtained in the range of 45 to 92 μm from morphological examination of all the prepared cryogel scaffolds using SEM micrographs. Scaffolds were found stable in aqueous medium (PBS, lysozyme containing solution DMEM medium) up to 12 days. Swelling study showed the superabsorbent nature of the SPI cryogels. All the fabricated

SPI cryogels had highly porous and interconnected pore morphology which facilitated quick absorption of blood and hence showed a better hemostatic effect than cotton and gauze. In the context of in vivo wound healing study in rat model, the favourable benefits of the SPI cryogel scaffolds manifested in terms of the quality of wound healing. All of these findings demonstrated that SPI cryogels possessed superior mechanical properties, such as good mechanical strength, high robustness, swift recovery, and stability. Thus the outcomes suggest that they may have the potential to be utilized as blood-triggered shape recovery hemostatic agents for the treatment of deep wound hemostasis. Cell culture results demonstrated that the manufactured SPI cryogel scaffolds had outstanding biocompatibility, with adequate cell attachment and proliferation. In 4% SPI samples, an excellent growth of 120% was seen after 4 days of culture. The outcomes of in vitro and in vivo studies indicate that the prepared soy protein scaffolds could be the potential material for skin substitution, wound healing, drug delivery and other various biomedical applications.

4.6 References

Abdel-Sayed, Philippe, Salim E. Darwiche, Ulrike Kettenberger, and Dominique P. Pioletti. 2014. "The Role of Energy Dissipation of Polymeric Scaffolds in the Mechanobiological Modulation of Chondrogenic Expression." *Biomaterials* 35 (6): 1890–97. https://doi.org/10.1016/j.biomaterials.2013.11.048.

Chatterjee, Cynthia, Stephen Gleddie, and Chao-Wu Xiao. 2018. "Soybean Bioactive Peptides and Their Functional Properties." *Nutrients* 10 (9): E1211. https://doi.org/10.3390/nu10091211.

Chen, Chih-Hao, Chang-Yi Kuo, Yan-Jie Wang, and Jyh-Ping Chen. 2016. "Dual Function of Glucosamine in Gelatin/Hyaluronic Acid Cryogel to Modulate Scaffold Mechanical Properties and to Maintain Chondrogenic Phenotype for Cartilage Tissue Engineering." *International Journal of Molecular Sciences* 17 (11): 1957. https://doi.org/10.3390/ijms17111957.

Cooperman, L., and D. Michaeli. 1984a. "The Immunogenicity of Injectable Collagen. I. A 1-Year Prospective Study." *Journal of the American Academy of Dermatology* 10 (4): 638–46. https://doi.org/10.1016/s0190-9622(84)80271-6.

Cooperman, L., and D. Michaeli. 1984b. "The Immunogenicity of Injectable Collagen. II. A Retrospective Review of Seventy-Two Tested and Treated Patients." *Journal of the American Academy of Dermatology* 10 (4): 647–51. https://doi.org/10.1016/s0190-9622(84)80272-8.

Curt, Sèverine, Muriel Subirade, and Mahmoud Rouabhia. 2009. "Production and In Vitro Evaluation of Soy Protein–Based Biofilms as a Support for Human Keratinocyte and Fibroblast Culture." *Tissue Engineering Part A* 15 (6): 1223–32. https://doi.org/10.1089/ten.tea.2008.0157.

Dainiak, Maria B., Iain U. Allan, Irina N. Savina, Lisa Cornelio, Elizabeth S. James, Stuart L. James, Sergey V. Mikhalovsky, Hans Jungvid, and Igor Yu Galaev. 2010. "Gelatin-Fibrinogen Cryogel Dermal Matrices for Wound Repair: Preparation, Optimisation and in Vitro Study." *Biomaterials* 31 (1): 67–76. https://doi.org/10.1016/j.biomaterials.2009.09.029.

DeFrates, Kelsey G., Robert Moore, Julia Borgesi, Guowei Lin, Thomas Mulderig, Vince Beachley, and Xiao Hu. 2018. “Protein-Based Fiber Materials in Medicine: A Review.” *Nanomaterials (Basel, Switzerland)* 8 (7): E457. https://doi.org/10.3390/nano8070457.

DeLustro, F., R. A. Condell, M. A. Nguyen, and J. M. McPherson. 1986. “A Comparative Study of the Biologic and Immunologic Response to Medical Devices Derived from Dermal Collagen.” *Journal of Biomedical Materials Research* 20 (1): 109–20. https://doi.org/10.1002/jbm.820200110.

Har-el, Yah-el, Jonathan A. Gerstenhaber, Ross Brodsky, Richard B. Huneke, and Peter I. Lelkes. 2014. “Electrospun Soy Protein Scaffolds as Wound Dressings: Enhanced Reepithelialization in a Porcine Model of Wound Healing.” *Wound Medicine* 5 (June): 9–15. https://doi.org/10.1016/j.wndm.2014.04.007.

He, Yujing, Chunhua Wang, Chenzhi Wang, Yuanhang Xiao, and Wei Lin. 2021. “An Overview on Collagen and Gelatin-Based Cryogels: Fabrication, Classification, Properties and Biomedical Applications.” *Polymers* 13 (14): 2299. https://doi.org/10.3390/polym13142299.

Huang, Xinxin, Chao Ma, Yecheng Xu, Jinfeng Cao, Jingchao Li, Jianzhang Li, Sheldon Q. Shi, and Qiang Gao. 2022. “A Tannin-Functionalized Soy Protein-Based Adhesive Hydrogel as a Wound Dressing.” *Industrial Crops and Products* 182 (August): 114945. https://doi.org/10.1016/j.indcrop.2022.114945.

Huang-Lee, L. L., D. T. Cheung, and M. E. Nimni. 1990. “Biochemical Changes and Cytotoxicity Associated with the Degradation of Polymeric Glutaraldehyde Derived Crosslinks.” *Journal of Biomedical Materials Research* 24 (9): 1185–1201. https://doi.org/10.1002/jbm.820240905.

Jao, Dave, Ye Xue, Jethro Medina, and Xiao Hu. 2017. “Protein-Based Drug-Delivery Materials.” *Materials* 10 (5): 517. https://doi.org/10.3390/ma10050517.

Jiang, L. -B., D. -H. Su, P. Liu, Y. -Q. Ma, Z. -Z. Shao, and J. Dong. 2018. “Shape-Memory Collagen Scaffold for Enhanced Cartilage Regeneration: Native Collagen versus Denatured Collagen.” *Osteoarthritis and Cartilage* 26 (10): 1389–99. https://doi.org/10.1016/j.joca.2018.06.004.

Jones, Vanessa, Joseph E Grey, and Keith G Harding. 2006. “Wound Dressings.” *BMJ : British Medical Journal* 332 (7544): 777–80.

Keefe, J., L. Wauk, S. Chu, and F. DeLustro. 1992. “Clinical Use of Injectable Bovine Collagen: A Decade of Experience.” *Clinical Materials* 9 (3–4): 155–62. https://doi.org/10.1016/0267-6605(92)90095-b.

Khabbaz, Bahareh, Atefeh Solouk, and Hamid Mirzadeh. 2019. “Polyvinyl Alcohol/Soy Protein Isolate Nanofibrous Patch for Wound-Healing Applications.” *Progress in Biomaterials* 8 (3): 185–96. https://doi.org/10.1007/s40204-019-00120-4.

Kim, Jong Oh, Jung Kil Park, Jeong Hoon Kim, Sung Giu Jin, Chul Soon Yong, Dong Xun Li, Jun Young Choi, et al. 2008. “Development of Polyvinyl Alcohol–Sodium Alginate Gel-Matrix-Based Wound Dressing System Containing Nitrofurazone.” *International Journal of Pharmaceutics* 359 (1): 79–86. https://doi.org/10.1016/j.ijpharm.2008.03.021.

Lee, Yong Kwon, Seung Yeul Kim, Ki Heon Kim, Bok-Hwan Chun, Kweon-Haeng Lee, Duk Jae Oh, and Namhyun Chung. 2008. “Use of Soybean Protein Hydrolysates for Promoting Proliferation of Human Keratinocytes in Serum-Free Medium.” *Biotechnology Letters* 30 (11): 1931–36. https://doi.org/10.1007/s10529-008-9796-0.

Liu, Huinan, Elliott B Slamovich, and Thomas J Webster. 2006. “Less Harmful Acidic Degradation of Poly(Lactic-Co-Glycolic Acid) Bone Tissue Engineering Scaffolds through Titania Nanoparticle Addition.” *International Journal of Nanomedicine* 1 (4): 541–45.

Liu, Yunqi, Dongmei Cai, Jing Yang, Yujie Wang, Xi Zhang, and Shengli Yin. 2014. “In Vitro Hemocompatibility Evaluation of Poly (4-Hydroxybutyrate) Scaffold.” *International Journal of Clinical and Experimental Medicine* 7 (5): 1233–43.

Lozinsky, Vladimir I. 2002. “Cryogels on the Basis of Natural and Synthetic Polymers: Preparation, Properties and Application.” *Russian Chemical Reviews* 71 (6): 489–511. https://doi.org/10.1070/RC2002v071n06ABEH000720.

Luo, Li-Hua, Yu-Feng Zhang, Xiao-Mei Wang, Yu Wan, Peter R. Chang, Debbie P. Anderson, and Yun Chen. 2010. “Preparation, Characterization, and In Vitro and In Vivo Evaluation of Cellulose/Soy Protein Isolate Composite Sponges.” *Journal of Biomaterials Applications* 24 (6): 503–26. https://doi.org/10.1177/0885328208099337.

Mano, J. F., G. A. Silva, H. S. Azevedo, P. B. Malafaya, R. A. Sousa, S. S. Silva, L. F. Boesel, et al. 2007. “Natural Origin Biodegradable Systems in Tissue Engineering and

Regenerative Medicine: Present Status and Some Moving Trends." *Journal of the Royal Society, Interface* 4 (17): 999–1030. https://doi.org/10.1098/rsif.2007.0220.

Mansur, Herman S., Carolina M. Sadahira, Adriana N. Souza, and Alexandra A. P. Mansur. 2008. "FTIR Spectroscopy Characterization of Poly (Vinyl Alcohol) Hydrogel with Different Hydrolysis Degree and Chemically Crosslinked with Glutaraldehyde." *Materials Science and Engineering: C*, Proceedings of the Symposium on Nanostructured Biological Materials, V Meeting of the Brazilian Materials Research Society (SBPMat), 28 (4): 539–48. https://doi.org/10.1016/j.msec.2007.10.088.

Mu, Changdao, Fang Liu, Qingsu Cheng, Hongli Li, Bo Wu, Guangzhao Zhang, and Wei Lin. 2010. "Collagen Cryogel Cross-Linked by Dialdehyde Starch." *Macromolecular Materials and Engineering* 295 (2): 100–107. https://doi.org/10.1002/mame.200900292.

Nagarajan, Sakthivel, Habib Belaid, Céline Pochat-Bohatier, Catherine Teyssier, Igor Iatsunskyi, Emerson Coy, Sébastien Balme, et al. 2017. "Design of Boron Nitride/Gelatin Electrospun Nanofibers for Bone Tissue Engineering." *ACS Applied Materials & Interfaces* 9 (39): 33695–706. https://doi.org/10.1021/acsami.7b13199.

Park, Eunkyo, Seung Min Lee, In-Kyung Jung, Yunsook Lim, and Jung-Hyun Kim. 2011. "Effects of Genistein on Early-Stage Cutaneous Wound Healing." *Biochemical and Biophysical Research Communications* 410 (3): 514–19. https://doi.org/10.1016/j.bbrc.2011.06.013.

Park, S. K., D. H. Bae, and K. C. Rhee. 2000. "Soy Protein Biopolymers Cross-Linked with Glutaraldehyde." *Journal of the American Oil Chemists' Society* 77 (8): 879–84. https://doi.org/10.1007/s11746-000-0140-3.

Patro, T. Umasankar, and H. Daniel Wagner. 2016. "Influence of Graphene Oxide Incorporation and Chemical Cross-Linking on Structure and Mechanical Properties of Layer-by-Layer Assembled Poly(Vinyl Alcohol)-Laponite Free-Standing Films." *Journal of Polymer Science Part B: Polymer Physics* 54 (22): 2377–87. https://doi.org/10.1002/polb.24226.

Peles, Zachi, and Meital Zilberman. 2012. "Novel Soy Protein Wound Dressings with Controlled Antibiotic Release: Mechanical and Physical Properties." *Acta Biomaterialia* 8 (1): 209–17. https://doi.org/10.1016/j.actbio.2011.08.022.

Qi, Xiaoliang, Xinyu Hu, Wei Wei, Hao Yu, Junjian Li, Jianfa Zhang, and Wei Dong. 2015. “Investigation of Salecan/Poly(Vinyl Alcohol) Hydrogels Prepared by Freeze/Thaw Method.” *Carbohydrate Polymers* 118 (March): 60–69. https://doi.org/10.1016/j.carbpol.2014.11.021.

Ramnath, Mr VARADARAJAN, Dr SANTHANAM Sekar, Dr SAMICKANNU Sankar, Dr Thotapalli, Parwathaleswara Sastry, and Dr ASIT BARAN Mandal. n.d. “IN VIVO EVALUATION OF COMPOSITE WOUND DRESSING MATERIAL CONTAINING SOYA PROTEIN AND SAGO STARCH” 4 (2): 6.

Reddy, Narendra, and Yiqi Yang. 2011. “Potential of Plant Proteins for Medical Applications.” *Trends in Biotechnology* 29 (10): 490–98. https://doi.org/10.1016/j.tibtech.2011.05.003.

Regal, J. F., D. G. Fraser, C. E. Weeks, and N. A. Greenberg. 2000. “Dietary Phytoestrogens Have Anti-Inflammatory Activity in a Guinea Pig Model of Asthma.” *Proceedings of the Society for Experimental Biology and Medicine. Society for Experimental Biology and Medicine (New York, N.Y.)* 223 (4): 372–78. https://doi.org/10.1046/j.1525-1373.2000.22353.x.

Santin, Matteo, Christopher Morris, Guy Standen, Luigi Nicolais, and Luigi Ambrosio. 2007. “A New Class of Bioactive and Biodegradable Soybean-Based Bone Fillers.” *Biomacromolecules* 8 (9): 2706–11. https://doi.org/10.1021/bm0703362.

Savina, Irina N., Mohamed Zoughaib, and Abdulla A. Yergeshov. 2021. “Design and Assessment of Biodegradable Macroporous Cryogels as Advanced Tissue Engineering and Drug Carrying Materials.” *Gels* 7 (3): 79. https://doi.org/10.3390/gels7030079.

Sharma, Archana, Sumrita Bhat, Tanushree Vishnoi, Vijayashree Nayak, and Ashok Kumar. 2013. “Three-Dimensional Supermacroporous Carrageenan-Gelatin Cryogel Matrix for Tissue Engineering Applications.” *BioMed Research International* 2013 (July): e478279. https://doi.org/10.1155/2013/478279.

Shingel, Kirill I., Liliana Di Stabile, Jean-Paul Marty, and Marie-Pierre Faure. 2006. “Inflammatory Inert Poly(Ethylene Glycol)--Protein Wound Dressing Improves Healing Responses in Partial- and Full-Thickness Wounds.” *International Wound Journal* 3 (4): 332–42. https://doi.org/10.1111/j.1742-481X.2006.00262.x.

Silva, C. L., D. Topgaard, V. Kocherbitov, J. J. S. Sousa, A. A. C. C. Pais, and E. Sparr. 2007. “Stratum Corneum Hydration: Phase Transformations and Mobility in Stratum Corneum, Extracted Lipids and Isolated Corneocytes.” *Biochimica et Biophysica Acta (BBA) - Biomembranes* 1768 (11): 2647–59. https://doi.org/10.1016/j.bbamem.2007.05.028.

Tie, Lu, Yu An, Jing Han, Yuan Xiao, Yilixiati Xiaokaiti, Shengjun Fan, Shaoqiang Liu, Alex F. Chen, and Xuejun Li. 2013. “Genistein Accelerates Refractory Wound Healing by Suppressing Superoxide and FoxO1/INOS Pathway in Type 1 Diabetes.” *The Journal of Nutritional Biochemistry* 24 (1): 88–96. https://doi.org/10.1016/j.jnutbio.2012.02.011.

Totea, Georgeta, Daniela Ionita, Ioana Demetrescu, and Mihaela Mitache. 2014. “In Vitro Hemocompatibility and Corrosion Behavior of New Zr-Binary Alloys in Whole Human Blood.” *Open Chemistry* 12 (7): 796–803. https://doi.org/10.2478/s11532-014-0535-1.

Tripathi, Anuj, Neeraj Kathuria, and Ashok Kumar. 2009. “Elastic and Macroporous Agarose-Gelatin Cryogels with Isotropic and Anisotropic Porosity for Tissue Engineering.” *Journal of Biomedical Materials Research. Part A* 90 (3): 680–94. https://doi.org/10.1002/jbm.a.32127.

Tripathi, Anuj, and Jose Savio Melo. 2019. “Cryostructurization of Polymeric Systems for Developing Macroporous Cryogel as a Foundational Framework in Bioengineering Applications.” *Journal of Chemical Sciences* 131 (9): 92. https://doi.org/10.1007/s12039-019-1670-1.

Van Vlierberghe, Sandra, Veerle Cnudde, Peter Dubruel, Bert Masschaele, An Cosijns, Ilse De Paepe, Patric J. S. Jacobs, Luc Van Hoorebeke, Jean Paul Remon, and Etienne Schacht. 2007. “Porous Gelatin Hydrogels: 1. Cryogenic Formation and Structure Analysis.” *Biomacromolecules* 8 (2): 331–37. https://doi.org/10.1021/bm060684o.

Varshney, Neelima, Ajay Kumar Sahi, Suruchi Poddar, and Sanjeev Kumar Mahto. 2020. “Soy Protein Isolate Supplemented Silk Fibroin Nanofibers for Skin Tissue Regeneration: Fabrication and Characterization.” *International Journal of Biological Macromolecules* 160 (October): 112–27. https://doi.org/10.1016/j.ijbiomac.2020.05.090.

Weber, Marbod, Heidrun Steinle, Sonia Golombek, Ludmilla Hann, Christian Schlensak, Hans P. Wendel, and Meltem Avci-Adali. 2018. “Blood-Contacting Biomaterials: In

Vitro Evaluation of the Hemocompatibility." *Frontiers in Bioengineering and Biotechnology* 6. https://www.frontiersin.org/article/10.3389/fbioe.2018.00099.

Winter, George D. 1962. "Formation of the Scab and the Rate of Epithelization of Superficial Wounds in the Skin of the Young Domestic Pig." *Nature* 193 (4812): 293–94. https://doi.org/10.1038/193293a0.

Wong, Rachel Shet Hui, Mark Ashton, and Kalliopi Dodou. 2015. "Effect of Crosslinking Agent Concentration on the Properties of Unmedicated Hydrogels." *Pharmaceutics* 7 (3): 305–19. https://doi.org/10.3390/pharmaceutics7030305.

Yang, Gang, Zhenghua Xiao, Haiyan Long, Kunlong Ma, Junpeng Zhang, Xiaomei Ren, and Jiang Zhang. 2018. "Assessment of the Characteristics and Biocompatibility of Gelatin Sponge Scaffolds Prepared by Various Crosslinking Methods." *Scientific Reports* 8 (1): 1616. https://doi.org/10.1038/s41598-018-20006-y.

Yao, Chun-Hsu, Chia-Yu Lee, Chiung-Hua Huang, Yueh-Sheng Chen, and Kuo-Yu Chen. 2017. "Novel Bilayer Wound Dressing Based on Electrospun Gelatin/Keratin Nanofibrous Mats for Skin Wound Repair." *Materials Science and Engineering: C* 79 (October): 533–40. https://doi.org/10.1016/j.msec.2017.05.076.

Zhang, Jian, Xiaohang Fu, Wenhui Li, He Li, Zhiwei Ying, Xinqi Liu, and Liduan Yin. 2020. "Enhancement of Nutritional Soy Protein and Peptide Supplementation on Skin Repair in Rats." *Journal of Functional Foods* 75 (December): 104231. https://doi.org/10.1016/j.jff.2020.104231.

Zhao, Xin, Baolin Guo, Hao Wu, Yongping Liang, and Peter X. Ma. 2018. "Injectable Antibacterial Conductive Nanocomposite Cryogels with Rapid Shape Recovery for Noncompressible Hemorrhage and Wound Healing." *Nature Communications* 9 (1): 2784. https://doi.org/10.1038/s41467-018-04998-9.